

Feature learning in neural networks and kernel machines that recursively learn features

Adityanarayanan Radhakrishnan^{*,1}

Daniel Beaglehole^{*,3}

Parthe Pandit²

Mikhail Belkin^{2,3}

¹MIT, Broad Institute of MIT and Harvard.

²Hacıoğlu Data Science Institute, UC San Diego.

³Computer Science and Engineering, UC San Diego.

^{*}Equal contribution.

Abstract

Neural networks have achieved impressive results on many technological and scientific tasks. Yet, their empirical successes have outpaced our fundamental understanding of their structure and function. Identifying mechanisms driving the successes of neural networks can provide principled approaches for improving neural network performance and developing simple and effective alternatives. In this work, we isolate a key mechanism driving feature learning in fully connected neural networks by connecting neural feature learning to a statistical estimator known as average gradient outer product. We subsequently leverage this mechanism to design *Recursive Feature Machines* (RFMs), which are kernel machines that learn features. We show that RFMs (1) accurately capture features learned by deep fully connected neural networks, and (2) outperform a broad spectrum of models including neural networks on tabular data. Furthermore, we show how RFMs shed light on recently observed deep learning phenomena including grokking, lottery tickets, simplicity biases, and spurious features. We provide a Python implementation to make our method easily accessible.⁴

1 Introduction

In the last few years, modern neural networks have helped achieve major progress on a variety of applications including image generation [70], protein folding [89], and language understanding and generation [14]. Indeed, the impressive empirical successes of these complex models have recently far outpaced our fundamental understanding of their structure and function. Identifying key mechanisms driving the success of neural networks would lead to principled approaches for improving their performance and developing effective alternatives.

A major step toward understanding the structure of neural networks was the recent discovery that under certain conditions wide neural networks are equivalent to kernel machines [38]. Indeed, a number of unexpected generalization and optimization phenomena arising in neural networks can be understood through these simpler and more theoretically accessible models [10, 11, 57, 97]. Nevertheless, this connection with kernel machines has not been able to capture a key property of neural networks, which is their ability to “learn features”. This aspect of neural networks is thought to be a central contributor to their superior performance and is contrasted with a lack of feature learning in standard kernel machines [80, 99].

Yet, despite significant research efforts in this area, identifying the components of neural networks responsible for feature learning, or even its exact nature, has been a challenge. Different lines of investigation connect feature learning to various aspects of neural network methodology such as model capacity (e.g., network width/depth) [93], the initialization scheme [99], or the optimization method [50]. Given that infinitely wide neural networks are equivalent to kernel machines [38], several works argue that finite width

⁴[github.com/recursive-feature-machines](https://github.com/radhakrishnanaditya/recursive-feature-machines)

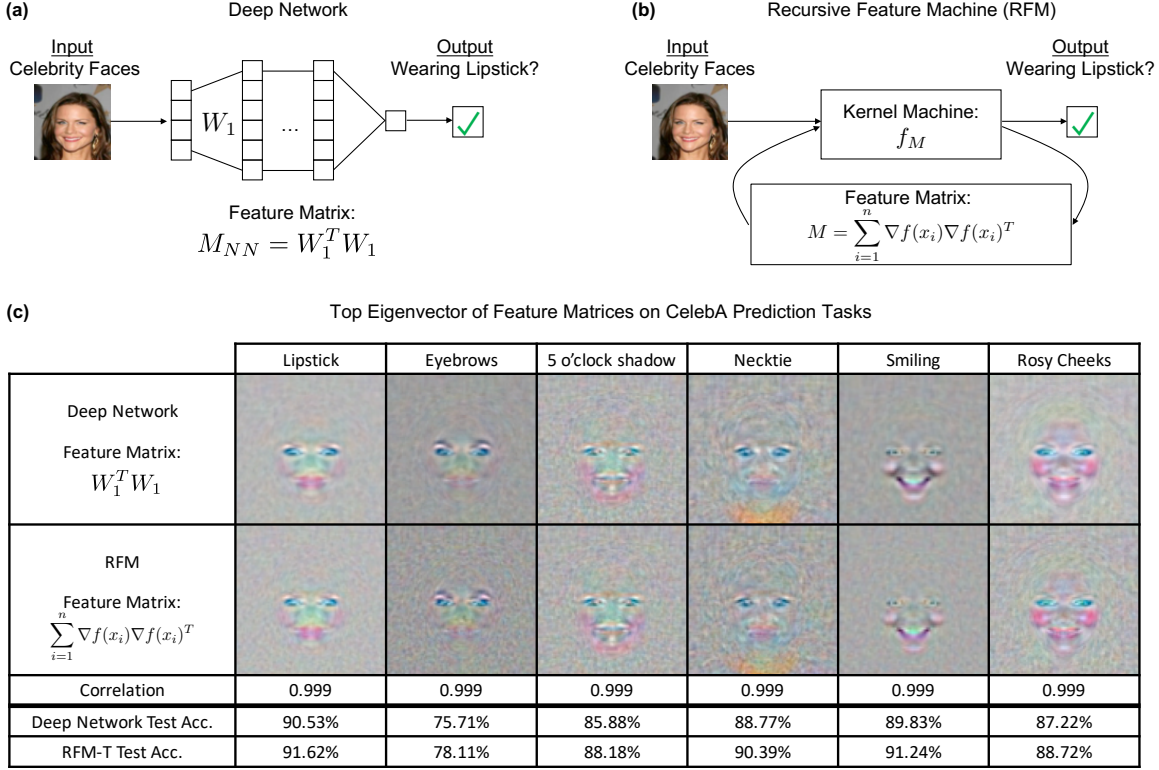


Figure 1: An overview of our main results. (a) We identify the feature matrix M_{NN} , which is given by the product of the transpose of the first layer weight matrix, W_1 , with itself. The feature matrix captures the features used by the deep network for prediction. (b) By connecting the feature matrix from neural networks to the average gradient outer product, we construct a class of kernel machines that recursively learn features (RFMs). Training RFMs involves iteratively estimating a predictor with a kernel machine and then estimating features with the average gradient outer product. (c) RFMs accurately capture features learned by deep fully connected neural networks. The top eigenvector of feature matrices learned by such networks and RFMs are highly correlated (Pearson correlation of 0.999) and appear visually indistinguishable. Moreover, training a kernel machine after thresholding top features identified by RFMs (denoted RFM-T) leads to higher test accuracy over deep networks for these tasks.

analyses through perturbative methods [31, 71] or through higher order approximations [7, 35] are needed to capture feature learning. In contrast, the work [99] argues that initializing networks near zero is key to learning features, regardless of model capacity. Furthermore, there is a line of work demonstrating that tuning the optimization method (in particular, increasing the learning rate) can improve the features learned by neural networks and ultimately improve their performance [47, 50, 107]. Another approach taken in works [63, 75, 105] analyzes neural networks from the point of view of non-parametric statistics and spline theory. Finally, several recent theoretical works characterize how neural networks learn features and identify relevant subspaces from data by studying the evolution of network layers during gradient descent [1, 22, 80]. As of the time of writing this paper, no conclusive unifying framework for feature learning has yet emerged.

In this work, we isolate a key mechanism of feature learning in deep fully connected neural networks by connecting feature learning with a statistical estimator for feature selection known in the literature as the *expected gradient outer product* [32, 88]. Furthermore, we posit that this is the primary mechanism behind feature learning in such neural networks. We subsequently leverage this connection to develop a class of kernel machines, *Recursive Feature Machines* (RFMs), that learn features by iteratively estimating expected gradient outer product. We demonstrate that RFMs (1) accurately capture features learned by deep networks, and (2) achieve state-of-the-art performance on tabular data, in particular outperforming a spectrum of machine learning models including modern neural networks. Hence, we argue that neural

networks are functionally equivalent to kernel machines with data-dependent kernels, a possibility discussed in [9] and observed in [53]. Finally, unlike neural networks, RFMs do not use backpropagation to learn features or construct predictors.

We provide theoretical evidence for the connection between feature learning in fully connected networks and the expected gradient outer product. In particular, under certain simplifying conditions on network initialization and training scheme, we show that the features learned in nonlinear, deep fully connected networks are equivalent to those given by expected gradient outer product.

In addition, we show that RFMs shed light on several striking phenomena recently identified in deep learning literature including

grokking [68], lottery tickets [26], simplicity biases [79], and spurious feature identification [82]. Thus, in addition to their practical value, we envision that RFMs will provide an analytically tractable framework for analyzing these phenomena and help improve interpretability of neural network predictors.

The mechanism driving feature learning in neural networks. In this work, we isolate a simple mathematical object that is key to capturing the features learned by the neural network through training, which we refer to as the *feature matrix* (See Fig. 1a). Letting $W_1 \in \mathbb{R}^{k \times d}$ denote the first layer weights in a fully connected network, this feature matrix is given by the Gram matrix $W_1^T W_1$. We connect the feature matrix learned by neural networks to the expected gradient outer product [88], which is a statistical estimator used for feature selection. We refer to this connection as the Neural Feature Ansatz. We provide extensive experimental evidence that (1) neural networks indeed learn features that are correlated to those given by the expected gradient outer product and (2) prediction using kernel machines on these features is competitive with and often surpasses performance of neural networks. We also provide theoretical evidence showing that, under certain conditions, the feature matrix at a given step of network training is equivalent to the expected gradient outer product of the neural network at that step. Lastly, our findings demonstrate that depth can amplify the features learned in the feature matrix, which improves predictors built on these features. Indeed, we conjecture that the main benefit of depth is this form of feature amplification.

Developing kernel machines that learn features. Kernel machines are classical machine learning models that are conceptually simple and are easy to implement computationally [77].

There has been renewed interest in these models since recent work [38] proved that under certain conditions on network initialization infinitely wide neural networks implement kernel machines using a Neural Tangent Kernel (NTK). Indeed, this equivalence holds for a broad class of neural network architectures [106]. The NTK has provided a simple and effective alternative to neural networks on a variety of tasks from image classification [3, 46] to virtual drug screening [69]. Yet, a fundamental limitation of the NTK and other classical kernel function choices is that they are not data adaptive, i.e., the choice of kernel function is fixed in advance before training. As a result, on certain tasks, kernel machines significantly underperform neural networks [22, 74, 99]. Recent works have analyzed so-called *after kernels* [53] extracted from neural networks *after* training, which are contrasted to NTKs obtained at initialization, *before* training. Kernel machines trained using after-kernels match the performance of neural networks, thereby suggesting that data-adaptive kernels can be as powerful as neural nets. Nevertheless, using after kernels is clearly impractical as their construction requires training a full neural network, thus obviating the need for another predictor.

In this work, we develop Recursive Feature Machines (RFM), which are a class of kernel machines that can learn features and are thus data-adaptive. RFMs contain a feature matrix that is iteratively refined via the average gradient outer product, thereby enabling feature learning (See Fig. 1b). RFMs consist of iterating a two step procedure where the first step involves estimating a predictor via a kernel machine and the second step involves using the average gradient outer product of the predictor obtained in the first step to update the feature matrix. Unlike neural networks, which generally have non-convex optimization landscapes, training RFMs involves iteratively solving a small number of convex (linear) optimization problems. Furthermore, the solution to each of these problems can be written in closed form. In addition to their simplicity, we show through extensive experimentation that the features learned by RFMs and deep networks are highly correlated. As an example, in Fig. 1c, we show that the features learned by RFMs and deep networks for prediction tasks from the CelebA dataset [52] have Pearson correlation of 0.999 for the top eigenvector of the feature matrix. Moreover, as exemplified in Fig. 1, training RFMs on these learned features leads to improved predictive performance compared to deep neural networks.

2 Neural Feature Learning and Recursive Feature Machines

We provide our main insight connecting feature learning in neural networks to the expected gradient outer product. This insight leads naturally to the development of recursive feature machines, which are a class of kernel machines that learn features. We begin by referencing the definition of expected and average gradient outer product from [88] below.⁵

Expected/Average Gradient Outer Product. Given a function $g : \mathbb{R}^d \rightarrow \mathbb{R}$ and data $x \in \mathbb{R}^d$ with density ρ , the *expected gradient outer product* is defined as

$$\mathcal{G}(g) = \mathbb{E}_x [\nabla g(x) \nabla g(x)^T] \in \mathbb{R}^{d \times d} \text{ with } \nabla g(x_i) := \nabla g(x)|_{x=x_i}.$$

As we typically do not have access to the density but rather samples $X = \{x_i\}_{i=1}^n \subset \mathbb{R}^d$, we approximate the above expectation via the *average gradient outer product* given by

$$\mathcal{G}_X(g) = \frac{1}{n} \sum_{i=1}^n \nabla g(x_i) \nabla g(x_i)^T.$$

We note that the expected gradient outer product can be thought of as a covariance matrix when the gradients have zero mean. Thus, in practice, we additionally consider centering gradients by subtracting the mean gradient prior to computing the outer products. We next introduce the feature matrix in neural networks, which we will subsequently connect to the expected gradient outer product above.

The Feature Matrix of a Neural Network. Let $W_1 \in \mathbb{R}^{k \times d}$ denote the first layer weights of a deep fully connected network. We define the *feature matrix* of the neural network f as $M_f \in \mathbb{R}^{d \times d}$, which has the form

$$M_f = W_1^T W_1.$$

Let $f^{(t)}$ denote the predictor learned by the network after t steps of gradient descent. Our main insight, which we call the Neural Feature Ansatz, is that

$$M_{f^{(t)}} \approx \mathcal{G}(f^{(t)}). \quad (\text{Neural Feature Ansatz})$$

The above ansatz should be viewed as a guiding principle. Before quantifying the approximation in the ansatz above and providing evidence for this claim, both theoretical and empirical, we first discuss its key implications. Suppose a neural network $f^{(t)}$, after t steps of optimization, generalizes well, i.e., $f^{(t)}$ is close to the optimal predictor f^* . In that case the Neural Feature Ansatz implies that $M_{f^{(t)}}$ is close to $\mathcal{G}(f^*)$. This, in turn, suggests that features learned by estimating $\mathcal{G}(f^*)$ should closely match those learned by well-performing neural networks. This observation implies that the neural networks learn features and a predictor simultaneously within the training process.

While the joint learning of features and the predictor from these features is a remarkable aspect of neural networks, there is no reason to believe that such simultaneous learning performed by neural networks is optimal. A more direct approach is to use an iterative two-step strategy that alternates between estimating the feature matrix and the predictor. Namely, given a candidate estimator \hat{f} , we can directly compute the corresponding feature matrix $\mathcal{G}(\hat{f})$ and then refine the estimator based on the newly learned features, iteratively. When this strategy is used in conjunction with kernel machines, we will refer to it as a recursive feature machine (RFM). We note this approach is closely related to the methodology developed in [88], which uses nearest neighbor methods for estimating predictors and features.

We now outline evidence for our main claim connecting the matrices $M_{f^{(t)}}$ and $\mathcal{G}(f^{(t)})$ for neural networks. Our two main lines of evidence are theoretical and empirical and are summarized below.

⁵For simplicity, we consider the gradient outer product of real-valued functions, but the gradient outer product naturally extends to functions that have multi-dimensional output by considering the product of the Jacobian and its transpose.

Theoretical Evidence. We identify several settings in Section 5 and Appendix A under which we prove that $M_{f^{(t)}} = \mathcal{G}(f^{(t)})$. In particular, we establish this result for deep nonlinear networks under the gradient independence ansatz, which has been commonly used to prove results in prior work [38] and established for networks with ReLU activation [3]. We further establish this equivalence for 1-hidden layer networks without this assumption (see Appendix A). See Table 1 in Section 5 for a summary of theoretical results in different settings.

Empirical Evidence. Our main line of empirical evidence is that the features learned by RFMs are highly correlated with those captured by the feature matrix $M_{f^{(t)}}$ of trained neural networks. In particular, the top eigenvectors of these matrices are essentially identical with Pearson correlation greater than 0.99. Furthermore, we show that predictors built by using our RFM features match or surpass performance of trained fully connected neural networks. Since the neural network feature matrix depends only on the first layer, this suggests that the first layer learns features relevant for prediction. In Section 6, we present evidence that increasing depth acts as a means of amplifying and improving these first layer features but does not appear to change the nature of feature learning in neural networks.

RFMs: a class of kernel machines that learn features. To alternate between estimating a predictor and learning features, we turn to a simple, effective, and well-studied class of models known as kernel machines [77]. Intuitively, training a kernel machine involves simply solving linear regression after applying a feature transformation on the data. Kernel machines are implemented using a kernel function [2], which is a positive semi-definite, symmetric function of two d -dimensional variables $K : \mathbb{R}^d \times \mathbb{R}^d \rightarrow \mathbb{R}$. Given a kernel function and a dataset $(X, y) \in \mathbb{R}^{d \times n} \times \mathbb{R}^{1 \times n}$, training a kernel machine gives a predictor, \hat{f} , of the form⁶

$$\hat{f}(x) = \hat{\alpha} K(X, x) \quad ; \quad \hat{\alpha} = y K(X, X)^{-1} ;$$

where $K(X, x) \in \mathbb{R}^n$ with $(K(X, x))_j = K(x_j, x)$ and $K(X, X) \in \mathbb{R}^{n \times n}$ with $(K(X, X))_{ij} = K(x_i, x_j)$. Further background on kernels including training kernel machines with ridge regularization is provided in Appendix B.

To develop kernel machines that learn features, we incorporate a positive semi-definite, symmetric matrix, M , as a learnable parameter into the kernel function. Namely, for radial kernel functions that depend only on the distance between points,⁷ e.g., $K(x, z) = \phi(\|x - z\|_2)$ for $\phi : \mathbb{R} \rightarrow \mathbb{R}$ and $x, z \in \mathbb{R}^d$, we incorporate the feature matrix by using the Mahanobis distance⁸

$$\|x - z\|_M^2 := (x - z)^T M (x - z).$$

Thus, we consider *Mahanobis kernels* of the form

$$K_M(x, z) := \phi(\|x - z\|_M). \quad (\text{Mahanobis kernel})$$

We now alternate between using kernel regression with the kernel function, K_M , to estimate a predictor and using the average gradient outer product to update the feature matrix, M . We refer to the model trained using this procedure as an RFM and present the general algorithm in Algorithm 1.

Note that this algorithm allows for a number of variations. One variation of RFMs that we found useful is thresholded RFMs (RFM-T), which involve re-training RFMs after thresholding to the top diagonal entries of M . We point out that training RFMs involves solving a small number of successive convex (linear) problems whose solutions can be written in a closed form. This is in contrast to the complexity of training deep neural networks, which involves non-convex optimization.

⁶When $K(X, X)$ is not invertible, we use the Moore-Penrose pseudoinverse, $K(X, X)^\dagger$, instead of $K(X, X)^{-1}$.

⁷We note that a similar modification can be made for general non-radial kernels by considering kernels $K_M(x, z) = K(M^{\frac{1}{2}}x, M^{\frac{1}{2}}z)$.

⁸We note that in statistical literature this distance is defined by $d_M(x, z) = \sqrt{(x - z)^T M^{-1} (x - z)}$ [56], but here, we make use of the notation from metric learning literature [13], which omits the inverse.

Algorithm 1 RFM

Input: X, y, K, T \triangleright Training features, X , training labels y , kernel function, K , and number of iterations, T
Output: α, M \triangleright Solution to kernel regression, α , and feature matrix, M
 $M = I_{d \times d}$ \triangleright Initialize M to be the identity matrix
for $t \in T$ **do**
 $K_{train} = K_M(X, X)$
 $\alpha = y K_{train}^{-1}$
 $M = \frac{1}{n} \sum_{x \in X} \nabla f(x) \nabla f(x)^T$ \triangleright Average gradient outer product of $f(x) = \alpha K_M(X, x)$
end for

While RFMs can be implemented with any kernel function, we mainly utilize the Laplace kernel due to its simplicity and empirical effectiveness.⁹ The Laplace kernel with bandwidth parameter L is defined as

$$K_M(x, z) = \exp\left(-\frac{\|x - z\|_M}{L}\right),$$

and its gradient¹⁰ has the form

$$\nabla_z K_M(x, z) = \frac{Mx - Mz}{L\|x - z\|_M} K_M(x, z).$$

We provide a memory efficient, vectorized implementation of gradient computation for the Laplace kernel in our code. Before providing empirical evidence demonstrating the effectiveness of RFMs, we discuss how the gradient outer product used in the RFM algorithm can give RFMs an advantage over standard kernel machines by maximizing alignment with the ideal kernel.

Maximizing kernel alignment through the gradient outer product. To improve kernel selection for supervised learning, a significant line of research (see, e.g., [20, 21, 83]) considered selecting a kernel or a combination of kernels to maximize alignment with the following “ideal” kernel function.

Definition 1. Suppose data $(x, f(x)) \in \mathbb{R}^d \times \mathbb{R}$ are generated by a target function $f(x)$. Then, the **ideal kernel** is $K^*(x, z) = f(x)f(z)$.

If one knows the target function f beforehand, then of course the ideal feature map is $\psi(x) = f(x)$, as the predictor $\mathbf{1}^T \psi(x)$ will recover the target value exactly (assuming no label noise). Further, in the Bayesian setting, the ideal kernel averaged over the distribution of target functions will be optimal [39]. We now showcase a benefit of the expected gradient outer product, M , by demonstrating that regression with a Mahanobis kernel using M will recover the ideal kernel when the target function is linear.

Proposition 1. Let $x \in \mathbb{R}^d$ have density ρ , let $\beta \in \mathbb{R}^d$, and consider the linear model, i.e., $f(x) = \beta^T x$. For $z, z' \in \mathbb{R}$, let $K_M(z, z') = z^T M z'$ with $M = \mathbb{E}_x[\nabla f(x) \nabla f(x)^T]$. Then, $K_M = K^*$.

Proof. Note $\nabla f(x) = \beta$ for all x . Hence, $M = \beta \beta^T$, and $K_M(z, z') = z^T \beta \beta^T z' = f(z)f(z') = K^*(z, z')$. \square

Moreover, the expected gradient outer product will provably reduce the sample complexity when the target function depends on only a few relevant directions in the data, as implied by the following proposition (proof in Appendix C).

Proposition 2. Let $x \in \mathbb{R}^d$ have density ρ and let the target function $f : \mathbb{R}^d \rightarrow \mathbb{R}$ be a polynomial with degree p and rank r , i.e., $f(x) = g(Ux)$ where $U \in \mathbb{R}^{r \times d}$ and $g : \mathbb{R}^r \rightarrow \mathbb{R}$. Let $M = \mathbb{E}_x[\nabla f(x) \nabla f(x)^T] \in \mathbb{R}^{d \times d}$. Then, there exists a fixed polynomial kernel such that kernel ridge regression on the transformed data $(M^{\frac{1}{2}}X, y)$ has the minimax sample dependence on rank, $O(r^p)$.

⁹We note also recent connection between Laplace kernels and the NTK [15, 28].

¹⁰While the Laplace kernel is not differentiable when the inputs to the kernel function are identical, we replace the gradient with zero at such points. This is equivalent to locally smoothing the kernel around the peak and is analogous to how deep network practitioners handle the non-differentiability of the rectified linear unit (ReLU) activation.

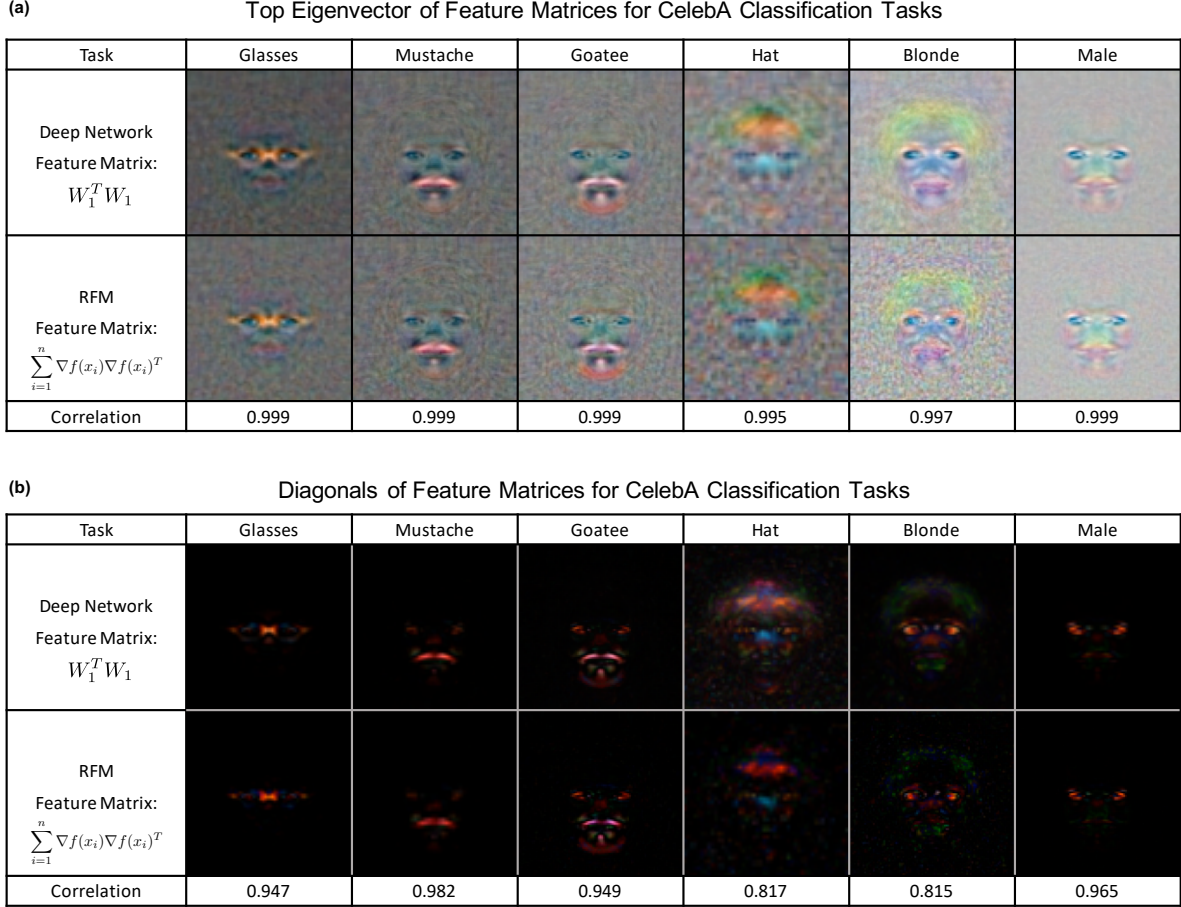


Figure 2: Comparison between feature matrices from RFMs and deep fully connected neural networks (denoted Deep Network) on CelebA prediction tasks. (a) The top eigenvector of the feature matrices from RFMs and deep networks visually highlights features related to the predictive task. These top eigenvectors are highly correlated (Pearson correlation greater than 0.99). (b) The diagonals of feature matrices from RFMs and deep networks highlight a sparse subset of features related to the predictive task. These diagonals are highly correlated (Pearson correlation greater than 0.8). Note that such high correlation is not due to sparsity since, for example, the correlation between the diagonals for glasses and mustache is only 0.110.

Remarks. This result is in contrast to using a fixed kernel for which $\Omega(d^p)$ samples are required to achieve better error than the trivial 0-function by kernel ridge regression [29]. While the above propositions assume we have knowledge of the expected gradient outer product of the target function, we note that related algorithms are optimal, even when the expected gradient outer product has not been estimated exactly. For example, kernel ridge regression using a Mahalanobis kernel with M set to the neural feature matrix after 1 step of gradient descent gives the optimal dependence on the rank r under certain conditions on the target function [22]. We note that a related iterative procedure using kernel smoothers to simultaneously estimate a predictor and gradients achieves minimax optimality for low-rank function estimation [34].

3 Empirical Results

We now present empirical evidence demonstrating that

1. Features learned by deep fully connected networks are accurately captured by RFMs (Section 3.1).
2. On real-world and synthetic datasets where feature learning is important, RFMs close the gap between

kernel machines and fully connected neural networks (Section 3.2).

3. RFMs provide state-of-the-art results on large tabular datasets and, in particular, outperform a spectrum of models including modern neural networks such as transformers and ResNets on a broad set of classification and regression tasks (Section 3.3).

All datasets, models, and training procedures are detailed in Appendix D.

3.1 RFMs accurately capture features learned by fully connected networks.

We present a striking series of examples illustrating the ability of RFMs to capture features from neural networks by comparing the features learned when using these models to predict attributes of celebrities from the CelebA dataset [52]. This dataset, commonly used for computer vision tasks, contains over 150,000 images of celebrity faces with each image labelled with up to 40 different attributes such as whether the individual is wearing glasses, smiling, has a mustache, etc. A description of the dataset and pre-processing methodology used in our experiments is provided in Appendix D. To avoid computational bottlenecks in comparing feature matrices of full resolution CelebA images, we downsample the images to have 96×96 resolution for our experiments.

In Fig. 2a and b, we visualize and compare the features matrices learned by fully connected networks and RFMs on a subset of six of predictive tasks in CelebA. In particular, in Fig. 2a, we visualize the top eigenvector of the feature matrix from deep neural networks and RFMs, and in Fig. 2b, we visualize the diagonals of these two feature matrices. Overall, we observe striking similarity between these learned features, which is corroborated by a high Pearson correlation (greater than 0.8) between the two sets of features. We note that the high correlation between the diagonals of the feature matrices is not due to the sparsity of the features. For example, the correlation between the diagonals of the feature matrices for glasses and mustache classification is 0.110. Top three eigenvectors and corresponding eigenvalues are presented in Appendix Fig. 15. In general, we observe that there is a large gap between the top eigenvalue and the second largest eigenvalue for both deep networks and feature matrices. This large gap and the similarity in the top eigenvector for deep network and RFM feature matrices further indicates that RFMs are accurately capturing features learned by deep networks.

3.2 RFMs close the gap between kernels and fully connected networks.

In addition to accurately capturing features learned by fully connected networks, RFMs surpass previous kernel methods in predictive performance and match or outperform neural networks in predictive performance. As an initial illustrative example, we consider the task of classifying street view house numbers (SVHN) [61]. As the SVHN classification task involves predicting the center digit in an image containing possibly multiple digits (see Fig. 3a), this task is naturally conducive to feature learning. Indeed, both deep networks and RFMs learn to subset to the center columns of the image as is shown by visualizing the diagonals of the feature matrix in Fig. 3b. Moreover, by learning to select this central region, RFMs and deep networks far outperform previous kernel methods with a gap of over 10% between these models and the classical Laplace kernel (see Fig. 2d). In addition to the real-world example of SVHN classification, RFMs additionally match or outperform neural networks on other illustrative tasks, including low rank polynomial regression identified by previous works [22, 93], where feature learning is important (see Appendix Fig. 16). In such low-rank polynomial settings, we also prove that transforming the data with the expected gradient outer product obtains an improvement in sample complexity (see Appendix C).

3.3 RFMs outperform neural networks and NTK on tabular data benchmarks.

We now demonstrate the remarkable effectiveness of RFMs in comparison with neural networks, NTK, and over 180 other classification methods on two tabular data benchmarks [23, 30]. Overall, we observe that RFMs achieve the best performance on these benchmarks across a variety of commonly used performance metrics.

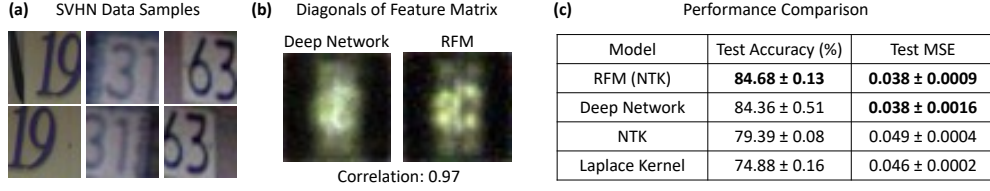


Figure 3: RFMs close the gap between kernel machines and deep fully connected networks on SVHN. (a) Samples from the SVHN dataset in which the goal is to identify the center digit from a view of potentially many digits. (b) Upon visualizing the diagonals of the feature matrices of RFMs and deep networks, we observe that these models learn to select the center digit. (c) By selecting the center digit, RFMs and deep networks provide a 10% increase in test accuracy over Laplace kernels and a 5% increase in test accuracy over NTKs. Using the NTK of a 1-hidden layer network on features learned by RFMs (denoted RFM (NTK)) leads to competitive test accuracy and test MSE with deep neural networks.

Tabular Benchmark 1 [23]. The first benchmark we consider is from [23], which compares the performance of 179 different machine learning methods on 121 tabular classification tasks. Recent works [4, 28] demonstrated that NTKs and variants of Laplace kernels (H- γ -exponential kernels) outperformed on a subset of 90 small datasets from the 121 that contained at most 5000 training examples. We will now demonstrate that RFMs outperform NTKs, variants of Laplace kernels, and all 179 other methods from [23] on the subset of 90 small datasets and the full 121 datasets from the original benchmark. In our analysis, we compare performance according to the following metrics used in [23] and in [4]:

- Friedman rank: The average rank of the classifier across all datasets.
- Average accuracy: The average accuracy of the classifier across all datasets.
- P90/P95: The percentage of datasets on which the classifier obtained accuracy within 90%/95% of that of the best performing model.
- PMA: The percentage of the maximum accuracy achieved by a classifier averaged across all datasets.

In Fig. 4a and b, we observe that RFMs outperform all previous methods across all metrics on both the subset of 90 small datasets and all 121 tasks. Moreover, we importantly note that while some of the datasets contain up to 130000 training examples, RFMs are computationally fast to train through the use of pre-conditioned linear system solvers such as EigenPro [54, 55].

In Fig. 4c, we compare the difference in error (100% - accuracy) between RFMs and the classical Laplace kernel, which is equivalent to an RFM where the feature matrix M is the identity matrix. In particular, we observe that the Laplace kernel generally results in high error than the RFM for larger datasets. In Fig. 4d, we report the relative decrease in error between RFMs and the Laplace kernel. We observe sizable improvement in relative error for larger datasets and those with higher dimensional data.

Tabular Benchmark 2 [30]. The second tabular benchmark we consider is from [30], which compares the performance of modern neural networks such as transformers [73, 85] against recent advances in tree-based models such as gradient boosted trees [17]. While this work has fewer “large” tabular datasets (those with greater than 10000 training samples), we again observe that RFMs generally outperform these modern tree-based models and neural networks.

In Fig. 5a and b, we compare RFMs to two transformer models [73, 85], ResNet [33], and two gradient boosting tree models [17, 65] across all “large” classification and regression tasks considered in [30]. Since there are only seven total large tasks in this benchmark, we report the accuracy on each task individually. Following [30], in Fig. 5c and c, we additionally report the average accuracy (R^2) for classification (regression), PMA, Friedman rank, and the average distance to the minimum (ADTM) for all models across all datasets. The ADTM metric accounts for varying dataset difficulty by normalizing the test accuracy for each task between 0 and 1 via min-max scaling across classifier performance. We observe that RFMs are the top

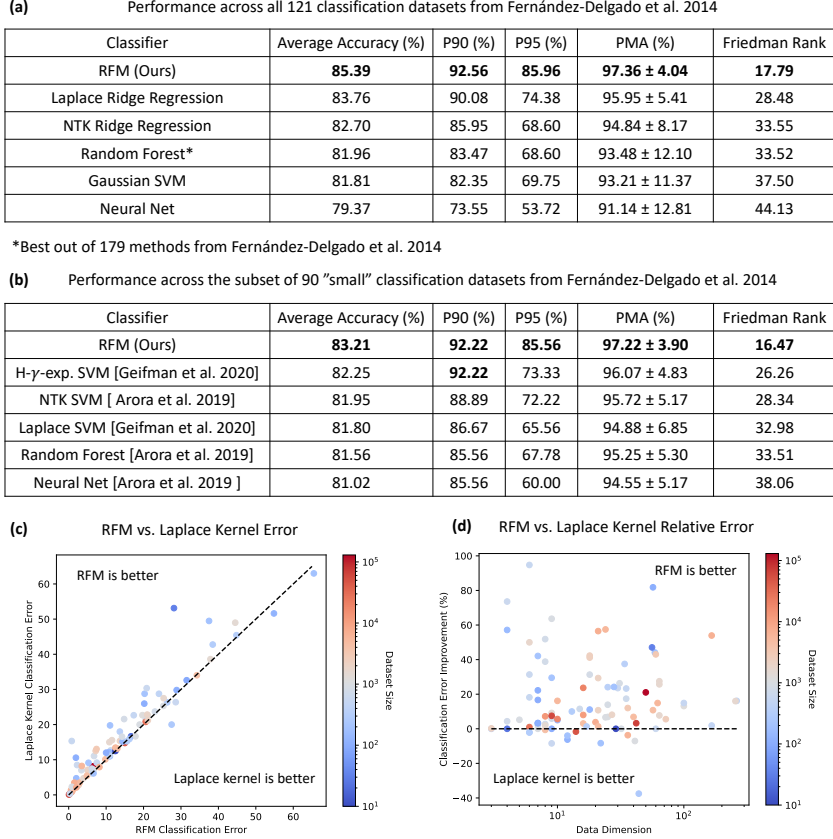


Figure 4: Comparison of 182 models including RFMs, NTKs, random forests, and fully connected neural networks on tabular datasets from [23]. All metrics, models, and training details are outlined in Appendices D and E. (a) Comparison between RFMs and 181 models on the 121 datasets from [23]. RFMs took 40 minutes to achieve these results while Neural Nets took 5 hours (both measurements are in wall time on a server with two Titan Xp GPUs). (b) Comparison between RFMs, NTKs [4], and variants of the Laplace kernel (H- γ -exp. SVM) on a subset of 90 classification tasks from [23] containing at most 5000 training examples. (c) We compare the error rate (100% - accuracy) between RFMs and Laplace kernels, which are equivalent to RFMs when the feature matrix is the identity matrix. (d) We report the relative decrease in error between RFMs and Laplace kernels, i.e., $100 \cdot \frac{\text{Error Laplace} - \text{Error RFM}}{\text{Error Laplace}}$, as a function of data dimension and size.

performing model on the majority of large classification and regression tasks. We also observe that RFMs achieve the highest on all metrics across all classification tasks, and are competitive with XGBoost across all regression tasks. RFMs outperform all neural network models on all classification and regression tasks. **Crucially, we used only 3600 compute hours for our method, while results with all other methods are with 20000 compute hours [30].** Further, for any fixed setting of data transformations, at most 650 compute hours of tuning were required over all tasks.

In Appendix Tables 2 and 3, we note that RFMs outperform modern neural networks and are competitive with tree-based models on “medium” size tabular datasets (fewer than 10000 training examples) considered in [30].¹¹ We note that this is in accordance with intuition since we would expect feature learning to be particularly beneficial on larger datasets, where the expected gradient outer product estimate is more accurate. In Tables 4 and 5, we present results for models on datasets that have categorically encoded data. Here, we again observe that RFMs generally provide an improvement over neural networks but are slightly outperformed by tree-based models on regression tasks.

¹¹In these tables, missing entries are denoted with a – and indicate that the result is not found in the logs provided by [30].

(a) Accuracy (%) across large classification datasets from Grinsztajin et al. 2022

Dataset	RFM	XGBoost	Gradient Boosting Tree	Resnet	SAINT	MLP	FT Transformer
MiniBooNE	94.97	94.47	94.14	94.61	94.32	94.32	94.56
HIGGS	72.44	72.87	72.55	72.39	72.75	71.15	73.13
Coverttype	94.10	89.74	89.76	89.39	89.59	87.43	90.69
Jannis	80.68	79.56	79.47	78.59	79.77	76.45	79.74

(b) R^2 across large regression datasets from Grinsztajin et al. 2022

Dataset	RFM	XGBoost	Gradient Boosting Tree	Resnet	SAINT	FT Transformer
Diamonds	0.948	0.948	0.947	0.941	0.945	0.945
NYC Taxi Green Dec. 2016	0.569	0.629	0.624	0.247	0.534	0.120
Year	0.334	0.307	0.307	0.119	0.289	0.117

(c) Metrics across all classification datasets from Grinsztajin et al. 2022

Metric	RFM	XGBoost	Gradient Boosting Tree	Random Forest	Resnet	SAINT	MLP	FT Transformer
Average Accuracy (%)	83.84	83.63	83.28	83.31	81.81	82.43	81.13	82.62
ADTM	0.810	0.762	0.641	0.555	0.286	0.458	0.089	0.549
PMA	0.991 ± 0.017	0.990 ± 0.014	0.986 ± 0.013	0.986 ± 0.010	0.967 ± 0.029	0.975 ± 0.026	0.959 ± 0.030	0.977 ± 0.026
Friedman rank	2.39	2.63	3.95	4.24	6.05	5.13	7.37	4.24

(d) Metrics across all regression datasets from Grinsztajin et al. 2022

Metric	RFM	XGBoost	Gradient Boosting Tree	Random Forest	Resnet	SAINT	FT Transformer
Average R^2	0.776	0.780	0.771	0.758	0.749	0.770	0.744
ADTM	0.701	0.823	0.534	0.322	0.489	0.572	0.504
PMA	0.984 ± 0.031	0.988 ± 0.023	0.974 ± 0.037	0.949 ± 0.083	0.928 ± 0.173	0.970 ± 0.042	0.919 ± 0.203
Friedman rank	3.00	2.13	4.00	5.52	4.52	4.30	4.52

Figure 5: Performance of RFMs, XGBoost, Gradient Boosting Trees, Random Forests, ResNets, Transformers (SAINT and FT), and fully connected networks (MLPs) from [30]. Our method used 3600 hours in total, while all other methods used 20000 hours for tuning, as reported in [30]. Results from all models other than RFMs are reported from the tables provided by [30]. All metrics and training details are outlined in Appendices D and E. Large tasks have 50000 training examples except for Jannis (40306 examples) and Diamonds (37758 examples). The medium tasks have at most 10000 samples. We show (a) average accuracy on large classification tasks and (b) average R^2 on large regression tasks. We compare model performance through commonly used metrics across all datasets for (c) classification, and (d) regression.

4 Deep Learning Phenomena through the Prism of RFM

Empirical studies of deep neural networks have brought to light a spectrum of phenomena, which are absent in analytically tractable kernel methods. In this section, we show that such phenomena are reproducible in RFMs, and we envision that RFMs will provide a framework for rigorous analysis of these phenomena. In particular, we discuss four specific phenomena below.

- The Lottery Ticket Hypothesis, Section 4.1.
- Grokking, Section 4.2.
- Inductive Bias of Deep Networks, Section 4.3.
- Spurious Feature Selection in Deep Networks, Section 4.4.

4.1 Lottery tickets in RFMs and deep networks.

Introduced in [26], the lottery ticket hypothesis refers to the claim that a randomly-initialized neural network contains a sub-network that can match or outperform the trained network when trained in isolation. The sparsity of feature matrices identified in this work provides direct evidence for this hypothesis. Indeed, such sparsity is immediately evident when visualizing the diagonals of the feature matrix as in Fig. 2b.

In line with the lottery ticket hypothesis, we demonstrate that retraining an RFM after thresholding coordinates of the data corresponding to these sparse regions in the feature matrix leads to a consistent increase in performance in many settings. In Fig. 6, we prune over 95% of pixels in CelebA images according to the features identified by RFMs and indeed, observe a consistent increase in predictive performance upon retraining a kernel on the thresholded features. We note that such thresholding drastically reduces

Lottery Tickets and RFMs







Task	Glasses	Mustache	Goatee	Eyebrows	Rosy Cheeks	Smiling
Thresholded RFM Features						
Percent of Pixels Remaining	1.42%	1.66%	3.40%	1.44%	2.43%	1.76%
RFM Accuracy	90.92%	88.15%	89.40%	74.36%	86.66%	89.62%
RFM-T Accuracy	94.06%	91.32%	91.19%	78.11%	88.72%	91.24%

Figure 6: Connections between lottery tickets in deep networks and RFMs. The diagonals of the feature matrices of RFMs trained on CelebA are sparse, thereby indicating that only a subset of coordinates is used for prediction. Such sparsity suggests that we can threshold to very few pixels while still minimally affecting performance. Indeed, by re-training RFMs upon thresholding to less than 3.5% of total pixels in CelebA tasks, performance consistently improves for these tasks.

computational and memory expenditure for the predictor both at test and run-time. Details regarding pruning thresholds are provided in Appendix D.

4.2 Grokking grokking

Introduced in recent work [68], grokking refers to the phenomena in which deep networks can begin to exhibit a dramatic increase in test accuracy when training past the point where training accuracy is 100%. While the work of [68] demonstrated this phenomenon in transformers trained on small algorithmic datasets, we demonstrate that both RFMs and deep fully connected networks can exhibit behavior similar to grokking.

We showcase this phenomenon by training neural networks and RFMs to classify between a subset of 96×96 resolution images of airplanes and trucks from the STL-10 dataset [18] (training details for RFMs and deep networks are presented in Appendix D). We modify this subset with two key features to enable grokking: (1) the dataset is small with a large class imbalance between the two classes with 500 examples of airplanes and 53 examples of trucks and (2) there is a small star of pixels in the upper left corner of each image that is colored white or black based on the class label (see Fig. 7a). The test set has no such class imbalance with 800 examples of each class.

Given the small size of the dataset, training only the last layer of a finite width networks with greater than 553 hidden units is sufficient for achieving 100% training accuracy. Indeed, as shown in Fig. 7b, we observe that the network rapidly approaches 100% training accuracy. Yet, when continuing to train the network, we observe that the test accuracy rises drastically from 80% to 99.38% in the last 120 epochs of training. This is due to the fact that the network learns the feature corresponding to the star during this stage of training (see inserts in Fig. 7b).

On the other hand, Fig. 7c demonstrates that RFMs also exhibit this phenomenon. Indeed, we find that kernel regression with the Laplace kernel (RFM at iteration 0) achieves 100% training accuracy but only 55.8% test accuracy since the feature matrix is the identity matrix. Yet, upon training the RFM for more iterations, we find that training accuracy remains at 100% but test accuracy rises to 100%. This is again since the RFM subsets the star pixels through more iterations (see inserts Fig. 7c).

4.3 Inductive biases of RFMs and deep networks.

A recent trend in deep learning is to use neural networks that are over-parameterized, i.e., capable of perfectly fitting training data. Despite their over-parameterization, such models yield improved performance [103]. To understand why such over-parameterized models generalize, recent works analyzed their inductive biases, i.e., properties of the predictor learned through training [5, 41, 62, 91]. Recent works [36, 79] have identified a particular form of inductive bias in deep networks, referred to as simplicity bias, where deep networks rely on simplest available features for classification.

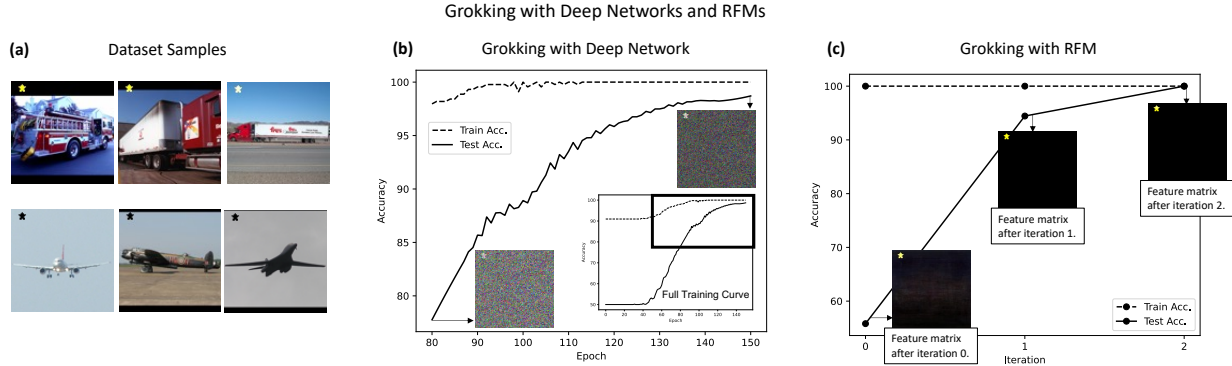


Figure 7: Grokking in fully connected networks and RFMs. (a) Corrupted samples from a subset of STL-10 in which a small star in the upper left indicates whether the image is a truck or an airplane. (b) A deep fully connected network with width larger than number of training samples quickly reaches near 100% training accuracy. Yet, as training continues past this point, the test accuracy rises drastically from 80% to 99.38%. Corresponding feature matrices (shown as inserts) indicate that test accuracy improved since the network has learned the star pixels that give away the class label. (c) While training accuracy is always 100% at all iterations of the RFM, iteration leads to a drastic rise in test accuracy from 55.8% to 100%. Again, feature matrices (shown as inserts) indicate that test accuracy improved since the RFM has learned the star pixels that give away the class label.

As an example, consider the experimental setup similar to that from [79] where we train a deep fully connected network on concatenated images of CIFAR-10 [44] and MNIST [45] with each CIFAR-10 class paired with a unique MNIST digit (see Fig. 8a). The work [79] showed through perturbative analyses that that neural networks trained on such a dataset relied only on the MNIST half of the concatenated image to make predictions, as, presumably, MNIST digits are “simpler” than CIFAR images. We show that the feature matrices of neural networks and RFMs both accurately capture such simplicity biases. In Fig. 8b, we visualize the diagonals of the feature matrices for the deep network and RFM. Both feature matrices indicate that these models are indeed learning to mask coordinates related to CIFAR-10 images and instead, focus on the MNIST digit for classification.

4.4 RFMs capture spurious features and biases in deep networks.

Recent works [37, 82] demonstrate that deep networks can leverage spurious features for prediction, which can make these models unreliable in mission-critical domains. In image classification, such features are those correlated with but not part of objects of interest. Examples include food co-occurring with plates or fingers co-occurring with band-aids [82]. It has also been argued [37] that such features are responsible for so-called “adversarial examples” [86], where small, often visually imperceptible alterations of images lead to dramatic loss of accuracy.

We now demonstrate that RFMs can serve as a useful tool for identifying spurious features used by deep networks during prediction. In particular, we showcase how such feature matrices can be used to identify spurious features leveraged by deep networks in CelebA lipstick and earring prediction tasks. In Fig. 9a, we observe that the diagonal of the RFM feature matrix indicates that eyes are unusually identified as a key feature for lipstick classification. Since eyes appear to be a spurious feature in RFMs and RFMs accurately capture neural network features, applying a small perturbation on these identified eye coordinates should lead to a large decrease in a network trained to predict lipstick. Indeed, we demonstrate this drop in accuracy in Fig. 9a. By replacing the eyes of all test images with those of a specific male, we see that the lipstick classification accuracy of a deep network drops from 90.53% to 55.23%. On the other hand, replacing the lips of all test images with those of the same male leads to only a small 4.87% drop in accuracy. We demonstrate a similar phenomenon for earring classification in Fig. 9b in which RFMs also identify eyes as a key feature for earring classification.

Simplicity Bias of Deep Networks and RFMs

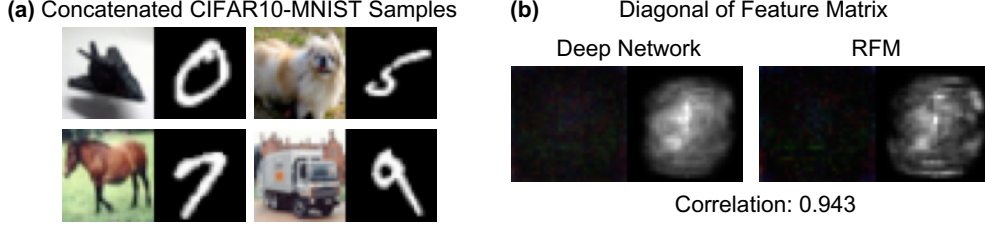


Figure 8: RFMs accurately capture inductive biases and in particular, simplicity biases of deep fully connected networks. (a) We train RFMs and neural networks on a dataset similar to that from [79] in which we concatenate images of CIFAR-10 objects with unique digits from MNIST. (b) Upon visualizing the diagonals of the feature matrices of trained deep networks and RFMs, we observe that both models learn to mask the CIFAR-10 image and focus on the MNIST digit for prediction.

5 Theoretical Evidence.

We now present theoretical evidence connecting feature learning in neural networks to the expected gradient outer product. We begin by proving that the neural feature matrix is equivalent to the expected gradient outer product of the trained network after gradient descent for deep ReLU networks where only the first layer is trained. We first introduce the relevant notation for deep neural networks.

Notation. Let $g : \mathbb{R}^d \rightarrow \mathbb{R}$ denote an L hidden layer network with element-wise activation $\phi : \mathbb{R} \rightarrow \mathbb{R}$ of the form:

$$g(x) = a^\top \phi_{(L)}(x) \quad \phi_{(\ell)}(x) = \begin{cases} \phi \left(\sqrt{\frac{c_\phi}{k_\ell}} W_\ell \phi_{(\ell-1)}(x) \right) & \ell \in \{1, \dots, L\} \\ x & \ell = 0 \end{cases} \quad (1)$$

where $a \in \mathbb{R}^{k_L}$ and $W_\ell \in \mathbb{R}^{k_\ell \times k_{\ell-1}}$ for $\ell \in [L]$ with $k_\ell \in \mathbb{Z}_+$ and $k_0 = d$. We denote row k of weight matrix W_ℓ by $W_{\ell,k} \in \mathbb{R}^{d \times 1}$.

Theorem 1 below (proof in Appendix A) establishes equivalence between the neural feature matrix and the expected gradient outer product for deep ReLU fully connected networks under the following gradient independence ansatz.

Gradient Independence Ansatz (GIA).¹² *In computing gradients, whenever we multiply by a weight matrix, W_ℓ , we can instead multiply by an i.i.d. copy without changing the gradient.*

We note that the GIA has been used in a range of works including [16, 66, 76, 96, 98, 100, 101] and is implicit in the original NTK derivation [38].¹³ In [3] the authors prove this ansatz for fully connected neural networks with ReLU activation functions.

Theorem 1 (Deep non-linear network). *Let g denote an L -hidden layer network with ReLU activation $\phi(z) = \max\{0, z\}$. Suppose W_1 is fixed and arbitrary (e.g., from training a neural network). Let $\{x_i, y_i\}_{i=1}^n \subset \mathbb{R}^d \times \mathbb{R}$. If $x \sim \mathcal{N}(0, I_d)$, then*

$$\frac{1}{k_1} W_1^\top W_1 = \mathbb{E}_x \left[\lim_{k_2, \dots, k_L \rightarrow \infty} \mathbb{E}_a \left[\nabla_x g(x) \nabla_x g(x)^\top \right] \right].$$


We note when the activation function is linear and W_1 is fixed or sampled independently of the outer layers, the gradient independence condition is not required for Theorem 1 to hold (see Appendix A). In










¹²This is usually called an assumption in the literature (e.g., Assumption 2.2 in [98]). We prefer the word *ansatz*, as this is a simplifying principle rather than a true mathematical assumption.

¹³This condition is required for establishing the closed form of the deep NTK presented in [38] as observed in [98] but is not needed to establish transition to linearity (e.g., [51]).

(a) Lipstick Classification

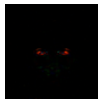
Diagonal of RFM Feature Matrix:



Corruption	Mask	Corrupted Samples		Test Acc.
None				90.53%
Lips (1260 Pixels)				85.66%
Eyes (477 Pixels)				55.32%

(b) Earring Classification

Diagonal of RFM Feature Matrix:



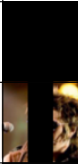








Corruption	Mask	Corrupted Samples		Test Acc.
None				76.11%
Ears (17280 Pixels)				71.58%
Eyes (426 Pixels)				53.25%

Figure 9: Feature matrices of RFMs capture spurious features learned by deep networks. (a, b) The diagonal of the feature matrix for an RFM trained on lipstick (or earring) classification unusually indicates that eyes are used as a key feature. We thus construct a mask based on the top RFM features and replace the eyes of all test samples with those of a single individual. A neural network trained on lipstick (or earring) classification does 35% (or 23%) worse on these corrupted samples. On the other hand, replacing the lips (or ears) of all test samples with those from the same individual leads to only a minor, 5%, decrease in accuracy.

Appendix A, we additionally prove that the neural feature matrix is equivalent to the expected gradient outer product of the trained network for 1-hidden layer networks without this assumption. A full outline of our theoretical results is presented in Table 1.

Result	Activation	Steps	Depth	Outer layer weights	Initialization	GIA Required
Theorem 1	ReLU	Any	Any	Fixed, i.i.d.	Any	Yes
Proposition 3	ReLU	Any	2	Re-sampled, i.i.d.	Any	No
Proposition 4	Linear	Any	2	Fixed, i.i.d.	Zero	No
Proposition 5	Linear	2 steps	2	Trainable, i.i.d	Zero	No

Table 1: Settings for which we theoretically connect the expected gradient outer product and neural network feature matrix. *Activation* refers the type of network activation function. *Steps* refers to the number of steps of gradient descent for which the proof holds. *Depth* refers to the depth of the neural network considered. *Outer layers* describes how the layers other than the first are initialized and trained. *Initialization* refers to the initialization method of the first layer weights. *GIA Required* indicates whether the gradient independence ansatz is required for the result to hold.

6 Feature amplification with depth.

We demonstrate that increasing network depth can improve the neural feature matrix by amplifying relevant features. In particular, depth can improve the predictor at initialization, thereby leading to an improved estimate of relevant features through the expected gradient outer product. Indeed, this process yields a positive feedback loop: the better the first-layer features, the better the learned predictor, and vice-versa. We note that such feature amplification does not preclude hierarchical feature learning. Nevertheless, we show that training a kernel machine on first layer features learned from a deep network is sufficient for

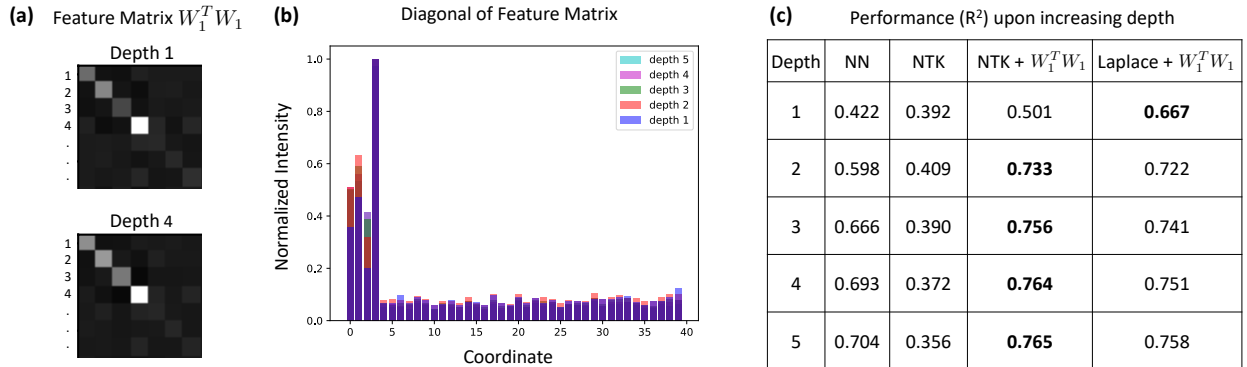


Figure 10: Low rank polynomial regression with data drawn from a Gaussian distribution, $x \sim \frac{1}{4}\mathcal{N}(0, I)$, and no label noise. 1000 train, validation, and test samples were used, and the target function is $f^*(x) = x_1 x_2 \cdot \mathbb{1}\{x_4 > 0\} + x_3 \cdot \mathbb{1}\{x_4 < 0\}$. Depth refers to the number of hidden layers. We compare performance across the following models: neural networks (NN), infinite width NTK upon varying depth (NTK), infinite width NTK with varying depth on top of deep neural feature matrices (NTK + $W_1^T W_1$), and Laplace kernel on top of deep neural feature matrices (Laplace + $W_1^T W_1$). We plot (a) the top-left corner of the neural feature matrix, along with (b) the normalized absolute values of the diagonal elements. In (c), we show the performance (R^2 values) of a fully connected network (NN), the NTK, and Mahalanobis NTK/Laplace kernels with the feature matrix from the neural network, as depth increases. Bold values indicate the best performance for each depth.

matching or surpassing network performance, thereby highlighting the importance of first layer features.

We present an example of feature amplification through depth for low rank polynomial regression in Fig. 10 and additional examples for low rank polynomial regression and SVHN image classification in Appendix F. In particular, we show that deep networks trained on these tasks are out-performed by using the Mahalanobis kernel, K_M , for $M = W_1^T W_1$, given by the empirical neural feature matrix. All experimental details are presented in Appendix D. Namely, in Fig. 10a and b, we observe that the neural feature matrix for a network with four hidden layers has higher intensity on the first four coordinates that are relevant for prediction than that of the one hidden layer network, which has higher intensity on non-relevant coordinates. Moreover, in Fig. 10c, we observe that the four hidden layer network achieves better performance on this task than the one hidden layer network. Lastly, we observe that Mahalanobis NTK and Laplace kernels modified with the neural feature matrix outperform neural networks of the same depth.

7 Summary, Discussion, and Outlook

Summary of results. In this work, we isolated a key mechanism of feature learning in deep fully connect neural networks. In particular, we posited the Neural Feature Ansatz, which states that the features learned by the first layer of fully connected networks are closely related to those given by the average gradient outer product. We provided evidence, both empirical and theoretical, for this claim and in particular, proved that the neural feature matrix is equal to the average gradient product for a number of settings (see Table 1). We subsequently leveraged the connection with the average gradient outer product to develop a simple class of kernel machines, Recursive Feature Machines (RFMs), that learn features. We demonstrated that RFMs are able to (1) accurately capture features learned by deep fully connected neural networks, and (2) yield state-of-the-art performance on large tabular datasets. Finally, we demonstrated that many intriguing phenomena of deep learning can be understood through the prism of our algorithm, as manifestations of alternating between feature selection and predictor construction.

Comments, connections and consequences. We now discuss connections between our results and machine learning literature as well as some implications of our results.

- *The role of width: Transition to linearity vs. feature learning.* Under the NTK initialization scheme, very wide neural networks undergo a transition to linearity and implement kernel regression with a kernel function that is not data adaptive and depends entirely on the network architecture [38, 51]. On the other hand, more narrow neural networks simultaneously learn both a predictor and features. Thus, network width modulates between two different regimes: one in which networks implement non-data-adaptive kernel predictors and another in which networks “learn features.” While this remarkable property highlights the flexibility of deep networks, it also illustrates their complexity. Indeed, simply increasing width under a particular initialization scheme increases the representational power of a neural network while decreasing its ability to learn features. In contrast, by separating predictor learning and feature learning into separate subroutines, RFMs are able to circumvent such modelling complexity without sacrificing performance.
- *The role of depth.* In this work, we connected feature learning in the first layer of deep fully connected networks with the expected gradient outer product. We further demonstrated that depth can amplify relevant features in the first layer of the network. Given that kernels trained on the RFM features match or surpass the performance of trained networks, we conjecture that the main practical benefits of depth are to amplify feature learning in the first layer. The remaining layers act as a kernel predictor over first layer features with deeper networks intuitively corresponding to “sharper”, more localized kernels. Whether feature learning in higher levels is significant for prediction (as argued in a range of works, e.g., [102]), remains an open question.
- *Interpretability.* A key area of practical interest is understanding and interpreting how neural networks make predictions. There is a rich literature on gradient-based methods for understanding features used by deep networks for image classification tasks [78, 81, 102]. These methods utilize gradients of trained networks to identify patterns in a given datum that are used by deep networks for classification. Rather than consider features important for any given sample, we show that the RFM feature matrix indicates the common subset of features used by fully connected networks on all samples. To highlight the impact of this finding, we identified that eyes were spurious features used by deep networks for classification of lipstick and earrings in the CelebA dataset (Fig. 9). We envision that the transparency provided by RFMs can serve as a key tool for increasing interpretability of machine learning models more generally.
- *Kernel alignment.* There is an extensive literature on learning data adaptive kernels for a given task by maximizing alignment with the “ideal” kernel [21, 95].
In the context of neural networks, [6] showed that as a neural network is trained, the empirical NTK increases alignment with the ideal kernel matrix. This is consistent with our result in Section 2 that the RFM using expected gradient outer product will maximize alignment for linear regression. It is an interesting direction for future work to identify whether RFMs or variants will approximate the ideal kernel under more general settings.
- *Empirical NTK.* Recently, a line of works have studied the connection between kernel learning and neural networks through the time-dependent evolution of the NTK [25]. An insightful work [53] showed that the *after kernel*, i.e. the empirical NTK at the end of training, matches the performance of the original network. Given the similarity in features learned between RFMs and neural networks, we believe that RFMs may be an effective means of approximating the after kernel without training neural networks.
- *Does feature learning always improve performance?* While we demonstrated that feature learning, both through RFMs and neural networks, can significantly improve performance on many tasks, it need not always lead to such improvements. In fact, previous work [4, 69] showed that non-feature-learning kernel methods outperformed corresponding neural networks on a variety of tasks and in particular, those involving small datasets. Moreover, from [23], we observed that the standard Laplace kernel (the non-feature learning, iteration 0 of RFM) was chosen as the best performing model during cross-validation on 45 out of 121 tabular datasets from [23]. It is, of course, possible that the specific data adaptation method used in RFM may not be optimal, and other methods would lead to improvements over the baseline on these datasets. Thus, an important direction of research is understanding the properties of data under which feature learning provides an advantage.

- *Connections to other statistical and machine learning methods.* Our approach has connections to a number of classical methods from statistics and machine learning. Below we briefly touch upon some of these connections.

- *Metric and manifold learning.* Updating the feature matrix in an RFM can also be viewed as learning a data-dependent Mahalanobis distance, i.e. a distance $d_M(x, z) = \sqrt{(x - z)^T M (x - z)}$ where M is the feature matrix. This connects to a large body of literature on metric learning with numerous applications to various supervised and unsupervised learning problems [13]. Furthermore, we believe that RFMs may benefit from incorporating ideas from the unsupervised and semi-supervised manifold learning and nonlinear dimensionality reduction literature [12, 72]. We also note that some of the early work on Radial Basis Networks explicitly addressed metric learning as a part of kernel function construction [67].
- *Supervised dimension reduction.* The problem of identifying key variables necessary to understand the response function (called sufficient dimensionality reduction in [48]) has been investigated in depth in the statistical literature. In particular, estimates of the gradient of the target function can be used to identify relevant coordinates for the target function. A series of works proposed methods that simultaneously learn the regression function and its gradient by non-parametric estimation [59, 60]. The gradients can then be used to improve performance on downstream prediction tasks [43]. Gradient estimation is particularly useful for coordinate selection in *multi-index models*, for which the regression function f^* has the form $f^*(x) = g(Ux)$, where U is a low rank matrix, as the gradients are restricted to the row-space of U . Similar to our method, the multi-index estimator in [34] iteratively identifies the relevant subspace by learning the regression function and its gradient, but makes use of kernel smoothers instead of kernel machines. Another line of work [49] estimates the Principal Hessian Directions, the eigenvectors of the average Hessian matrix of the target function, to identify relevant coordinates. Finally, a parallel line of research on “active subspace” methods in the context of *dynamical systems* has recently become a topic of active investigation [19].
- *FisherFaces and EigenFaces.* We further note the strong similarity between the eigenvectors of feature matrices (e.g., Figure 1) analyzed in this work and those given by EigenFace [84, 90], and FisherFace [8] algorithms. While EigenFaces are obtained in a purely unsupervised fashion, the FisherFace algorithm uses labeled images of faces and Fisher’s Linear Discriminant [24] to learn a linear subspace for dimensionality reduction. RFMs also learn linear subspaces based on labeled data but in a recursive way, using nonlinear classifiers.
- *Debiasing.* Debiasing is a statistical procedure of recent interest in the statistics literature [104]. Simply, given a high-dimensional problem with a hidden low-dimensional structure, a step of variable selection is performed by using methods such as Lasso [87] or sparse PCA [40]. A low-dimensional model is then fitted to the selected coordinates alone. We note that this procedure is similar to a single step of RFM. Indeed, RFM can be viewed as a non-linear iterative version of the debiasing procedure with soft coordinate selection.
- *Expectation Maximization (EM) and Boosting.* The RFM algorithm is reminiscent of the EM algorithm [58] with alternating estimation of the kernel predictor (M-step) and the feature matrix M (E-step). From this viewpoint, developing estimators for the feature matrix other than the sample covariance estimator considered in this work can be a productive research direction. Moreover, depending on properties of the data and the target function, the feature matrix may be structured. Such structure could be leveraged to develop more sample efficient estimators for the M-step. Somewhat similarly, RFMs are reminiscent of boosting [27] where a “weak learner”, only slightly correlated with the optimal predictor, is “boosted” by repeated application. In our context a suboptimal predictor can be iteratively improved as long as its average gradient outer product estimate is above the noise level.

Looking forward. Neural networks trained by gradient-based optimization methods have remarkable properties, which are still not fully understood. One of their particularly interesting aspects is the ability to learn a predictor and features at the same time in the process of training. Yet, there is no reason to believe that such simultaneous learning is optimal. Indeed, in this work, by decoupling feature learning

and predictor learning, we constructed effective algorithms that outperform neural networks on a variety of generalization tasks and are also far easier to train. In particular, the effectiveness of Recursive Feature Machines demonstrates that feature learning does not require backpropagation.

In our view, separating predictor and feature learning components of neural networks provides a path forward to modular algorithms that are easier to design, implement, and analyze theoretically, as well as to improvements of neural networks.

Acknowledgements

A.R. is supported by the Eric and Wendy Schmidt Center at the Broad Institute. A.R. thanks Caroline Uhler for support on this work, and A.R., M.B. thank her for many insightful discussions over the years. We are grateful to Phil Long for useful insight into centering the expected gradient outer product. We thank Daniel Hsu, Joel Tropp and Jason Lee for valuable literature references. We acknowledge support from the National Science Foundation (NSF) and the Simons Foundation for the Collaboration on the Theoretical Foundations of Deep Learning¹⁴ through awards DMS-2031883 and #814639 as well as the TILOS institute (NSF CCF-2112665). This work used the programs (1) XSEDE (Extreme science and engineering discovery environment) which is supported by NSF grant numbers ACI-1548562, and (2) ACCESS (Advanced cyberinfrastructure coordination ecosystem: services & support) which is supported by NSF grants numbers #2138259, #2138286, #2138307, #2137603, and #2138296. Specifically, we used the resources from SDSC Expanse GPU compute nodes, and NCSA Delta system, via allocations TG-CIS220009.

References

- [1] E. Abbe, E. Boix-Adsera, and T. Misiakiewicz. The merged-staircase property: a necessary and nearly sufficient condition for sgd learning of sparse functions on two-layer neural networks. In *Conference on Learning Theory*, pages 4782–4887. PMLR, 2022.
- [2] N. Aronszajn. Theory of reproducing kernels. *Transactions of the American mathematical society*, 68(3):337–404, 1950.
- [3] S. Arora, S. S. Du, W. Hu, Z. Li, R. Salakhutdinov, and R. Wang. On exact computation with an infinitely wide neural net. In *Advances in Neural Information Processing Systems*, 2019.
- [4] S. Arora, S. S. Du, Z. Li, R. Salakhutdinov, R. Wang, and D. Yu. Harnessing the power of infinitely wide deep nets on small-data tasks. In *International Conference on Learning Representations*, 2020.
- [5] D. Arpit, S. Jastrzębski, N. Ballas, D. Krueger, E. Bengio, M. S. Kanwal, T. Maharaj, A. Fischer, A. Courville, Y. Bengio, et al. A closer look at memorization in deep networks. In *International Conference on Machine Learning*, 2017.
- [6] A. Atanasov, B. Bordelon, and C. Pehlevan. Neural networks as kernel learners: The silent alignment effect. In *International Conference on Learning Representations*, 2022.
- [7] Y. Bai and J. D. Lee. Beyond linearization: On quadratic and higher-order approximation of wide neural networks. In *International Conference on Learning Representations*, 2019.
- [8] P. N. Belhumeur, J. P. Hespanha, and D. J. Kriegman. Eigenfaces vs. Fisherfaces: Recognition using class specific linear projection. *IEEE Transactions on pattern analysis and machine intelligence*, 19(7):711–720, 1997.
- [9] M. Belkin. Fit without fear: remarkable mathematical phenomena of deep learning through the prism of interpolation. *Acta Numerica*, 30:203–248, 2021.

¹⁴<https://deepfoundations.ai/>

- [10] M. Belkin, D. Hsu, S. Ma, and S. Mandal. Reconciling modern machine-learning practice and the classical bias–variance trade-off. *Proceedings of the National Academy of Sciences*, 116(32):15849–15854, 2019.
- [11] M. Belkin, S. Ma, and S. Mandal. To understand deep learning we need to understand kernel learning. In *International Conference on Machine Learning*, pages 541–549. PMLR, 2018.
- [12] M. Belkin and P. Niyogi. Laplacian eigenmaps for dimensionality reduction and data representation. *Neural computation*, 15(6):1373–1396, 2003.
- [13] A. Bellet, A. Habrard, and M. Sebban. Metric learning. *Synthesis lectures on artificial intelligence and machine learning*, 9(1):1–151, 2015.
- [14] T. Brown, B. Mann, N. Ryder, M. Subbiah, J. Kaplan, P. Dhariwal, A. Neelakantan, P. Shyam, G. Sastry, A. Askell, S. Agarwal, A. Herbert-Voss, G. Krueger, T. Henighan, R. Child, A. Ramesh, D. Ziegler, J. Wu, C. Winter, and D. Amodei. Language models are few-shot learners. In *Advances in Neural Information Processing Systems*, 2020.
- [15] L. Chen and S. Xu. Deep Neural Tangent Kernel and Laplace kernel have the same RKHS. In *International Conference on Learning Representations*, 2021.
- [16] M. Chen, J. Pennington, and S. Schoenholz. Dynamical isometry and a mean field theory of rnns: Gating enables signal propagation in recurrent neural networks. In *International Conference on Machine Learning*, pages 873–882. PMLR, 2018.
- [17] T. Chen and C. Guestrin. XGBoost: A scalable tree boosting system. In *Proceedings of the 22nd ACM SIGKDD International Conference on Knowledge Discovery and Data Mining*, pages 785–794. ACM, 2016.
- [18] A. Coates, H. Lee, and A. Y. Ng. An analysis of single layer networks in unsupervised feature learning. In *International Conference on Artificial Intelligence and Statistics*, 2011.
- [19] P. G. Constantine. *Active subspaces: Emerging ideas for dimension reduction in parameter studies*. SIAM, 2015.
- [20] C. Cortes, M. Mohri, and A. Rostamizadeh. Algorithms for learning kernels based on centered alignment. *The Journal of Machine Learning Research*, 13:795–828, 2012.
- [21] N. Cristianini, J. Shawe-Taylor, A. Elisseeff, and J. Kandola. On kernel-target alignment. *Advances in Neural Information Processing Systems*, 14, 2001.
- [22] A. Damian, J. Lee, and M. Soltanolkotabi. Neural networks can learn representations with gradient descent. In *Conference on Learning Theory*, pages 5413–5452. PMLR, 2022.
- [23] M. Fernández-Delgado, E. Cernadas, S. Barro, and D. Amorim. Do we need hundreds of classifiers to solve real world classification problems? *The Journal of Machine Learning Research*, 15(1):3133–3181, 2014.
- [24] R. A. Fisher. The statistical utilization of multiple measurements. *Annals of eugenics*, 8(4):376–386, 1938.
- [25] S. Fort, G. K. Dziugaite, M. Paul, S. Kharaghani, D. M. Roy, and S. Ganguli. Deep learning versus kernel learning: an empirical study of loss landscape geometry and the time evolution of the neural tangent kernel. *Advances in Neural Information Processing Systems*, 33:5850–5861, 2020.
- [26] J. Frankle and M. Carbin. The lottery ticket hypothesis: Finding sparse, trainable neural networks. In *International Conference on Learning Representations*, 2019.
- [27] Y. Freund and R. E. Schapire. A decision-theoretic generalization of on-line learning and an application to boosting. *Journal of computer and system sciences*, 55(1):119–139, 1997.

- [28] A. Geifman, A. Yadav, Y. Kasten, M. Galun, D. Jacobs, and B. Ronen. On the similarity between the laplace and neural tangent kernels. In *Advances in Neural Information Processing Systems*, 2020.
- [29] B. Ghorbani, S. Mei, T. Misiakiewicz, and A. Montanari. Linearized two-layers neural networks in high dimension. *The Annals of Statistics*, 49(2):1029–1054, 2021.
- [30] L. Grinsztajn, E. Oyallon, and G. Varoquaux. Why do tree-based models still outperform deep learning on typical tabular data? In *Neural Information Processing Systems Datasets and Benchmarks*, 2022.
- [31] B. Hanin and M. Nica. Finite depth and width corrections to the Neural Tangent Kernel. In *International Conference on Learning Representations*, 2020.
- [32] W. Härdle and T. M. Stoker. Investigating smooth multiple regression by the method of average derivatives. *Journal of the American statistical Association*, 84(408):986–995, 1989.
- [33] K. He, X. Zhang, S. Ren, and J. Sun. Deep residual learning for image recognition. In *Computer Vision and Pattern Recognition*, 2016.
- [34] M. Hristache, A. Juditsky, J. Polzehl, and V. Spokoiny. Structure adaptive approach for dimension reduction. *Annals of Statistics*, pages 1537–1566, 2001.
- [35] J. Huang and H.-T. Yau. Dynamics of deep neural networks and neural tangent hierarchy. In *International Conference on Machine Learning*, pages 4542–4551. PMLR, 2020.
- [36] M. Huh, H. Mobahi, R. Zhang, B. Cheung, P. Agrawal, and P. Isola. The low-rank simplicity bias in deep networks. *arXiv preprint arXiv:2103.10427*, 2021.
- [37] A. Ilyas, S. Santurkar, D. Tsipras, L. Engstrom, B. Tran, and A. Madry. Adversarial examples are not bugs, they are features. In *Advances in Neural Information Processing Systems*, 2019.
- [38] A. Jacot, F. Gabriel, and C. Hongler. Neural Tangent Kernel: Convergence and generalization in neural networks. In *Advances in Neural Information Processing Systems*, 2018.
- [39] A. Jacot, B. Simsek, F. Spadaro, C. Hongler, and F. Gabriel. Kernel alignment risk estimator: Risk prediction from training data. *Advances in Neural Information Processing Systems*, 33:15568–15578, 2020.
- [40] J. Janková and S. van de Geer. De-biased sparse PCA: Inference for eigenstructure of large covariance matrices. *IEEE Transactions on Information Theory*, 67(4):2507–2527, 2021.
- [41] D. Kalimeris, G. Kaplun, P. Nakkiran, B. Edelman, T. Yang, B. Barak, and H. Zhang. SGD on neural networks learns functions of increasing complexity. *Advances in neural information processing systems*, 32, 2019.
- [42] D. P. Kingma and J. Ba. Adam: A method for stochastic optimization. In *International Conference on Learning Representations*, 2015.
- [43] S. Kpotufe, A. Boularias, T. Schultz, and K. Kim. Gradients weights improve regression and classification. *Journal of Machine Learning Research*, 2016.
- [44] A. Krizhevsky. Learning multiple layers of features from tiny images. Master’s thesis, University of Toronto, 2009.
- [45] Y. LeCun, L. Bottou, Y. Bengio, and P. Haffner. Gradient-based learning applied to document recognition. *Proceedings of the Institute of Electrical and Electronics Engineers*, 86(11):2278–2324, 1998.
- [46] J. Lee, S. Schoenholz, J. Pennington, B. Adlam, L. Xiao, R. Novak, and J. Sohl-Dickstein. Finite versus infinite neural networks: an empirical study. In *Advances in Neural Information Processing Systems*, 2020.

- [47] A. Lewkowycz, Y. Bahri, E. Dyer, J. Sohl-Dickstein, and G. Gur-Ari. The large learning rate phase of deep learning: the catapult mechanism. *arXiv preprint arXiv:2003.02218*, 2020.
- [48] B. Li. *Sufficient dimension reduction: Methods and applications with R*. Chapman and Hall/CRC, 2018.
- [49] K.-C. Li. On principal hessian directions for data visualization and dimension reduction: Another application of stein’s lemma. *Journal of the American Statistical Association*, 87(420):1025–1039, 1992.
- [50] Y. Li, C. Wei, and T. Ma. Towards explaining the regularization effect of initial large learning rate in training neural networks. In *Advances in Neural Information Processing Systems*, volume 32, 2019.
- [51] C. Liu, L. Zhu, and M. Belkin. On the linearity of large non-linear models: when and why the tangent kernel is constant. In *Advances in Neural Information Processing Systems*, 2020.
- [52] Z. Liu, P. Luo, X. Wang, and X. Tang. Deep learning face attributes in the wild. In *Proceedings of International Conference on Computer Vision (ICCV)*, 2015.
- [53] P. M. Long. Properties of the after kernel. *arXiv preprint arXiv:2105.10585*, 2021.
- [54] S. Ma and M. Belkin. Diving into the shallows: a computational perspective on large-scale shallow learning. In *Advances in Neural Information Processing Systems*, 2017.
- [55] S. Ma and M. Belkin. Kernel machines that adapt to GPUs for effective large batch training. In *Conference on Machine Learning and Systems*, 2019.
- [56] P. C. Mahalanobis. On the generalized distance in statistics. In *Proceedings of the National Institute of Science of India*, 1936.
- [57] S. Mei and A. Montanari. The generalization error of random features regression: Precise asymptotics and the double descent curve. *Communications on Pure and Applied Mathematics*, 75(4):667–766, 2022.
- [58] T. K. Moon. The expectation-maximization algorithm. *IEEE Signal processing magazine*, 13(6):47–60, 1996.
- [59] S. Mukherjee and Q. Wu. Estimation of gradients and coordinate covariation in classification. *The Journal of Machine Learning Research*, 7:2481–2514, 2006.
- [60] S. Mukherjee, D.-X. Zhou, and J. Shawe-Taylor. Learning coordinate covariances via gradients. *Journal of Machine Learning Research*, 7(3), 2006.
- [61] Y. Netzer, T. Wang, A. Coates, A. Bissacco, B. Wu, and A. Y. Ng. Reading digits in natural images with unsupervised feature learning. *Advances in Neural Information Processing Systems (NIPS)*, 2011.
- [62] B. Neyshabur, R. Tomioka, and N. Srebro. In search of the real inductive bias: On the role of implicit regularization in deep learning. In *International Conference on Learning Representations Workshop Contribution*, 2015.
- [63] R. Parhi and R. D. Nowak. What kinds of functions do deep neural networks learn? insights from variational spline theory. *SIAM Journal on Mathematics of Data Science*, 4(2):464–489, 2022.
- [64] A. Paszke, S. Gross, F. Massa, A. Lerer, J. Bradbury, G. Chanan, T. Killeen, Z. Lin, N. Gimelshein, L. Antiga, A. Desmaison, A. Kopf, E. Yang, Z. DeVito, M. Raison, A. Tejani, S. Chilamkurthy, B. Steiner, L. Fang, J. Bai, and S. Chintala. Pytorch: An imperative style, high-performance deep learning library. In *Advances in Neural Information Processing Systems*, 2019.

- [65] F. Pedregosa, G. Varoquaux, A. Gramfort, V. Michel, B. Thirion, O. Grisel, M. Blondel, P. Prettenhofer, R. Weiss, V. Dubourg, J. Vanderplas, A. Passos, D. Cournapeau, M. Brucher, M. Perrot, and E. Duchesnay. Scikit-learn: Machine Learning in Python. *Journal of Machine Learning Research (JMLR)*, 12:2825–2830, 2011.
- [66] J. Pennington, S. Schoenholz, and S. Ganguli. Resurrecting the sigmoid in deep learning through dynamical isometry: theory and practice. *Advances in neural information processing systems*, 30, 2017.
- [67] T. Poggio and F. Girosi. Networks for approximation and learning. *Proceedings of the IEEE*, 78(9):1481–1497, 1990.
- [68] A. Power, Y. Burda, H. Edwards, I. Babuschkin, and V. Misra. Grokking: Generalization beyond overfitting on small algorithmic datasets. In *International Conference on Learning Representations Mathematical Reasoning in General Artificial Intelligence Workshop*, 2022.
- [69] A. Radhakrishnan, G. Stefanakis, M. Belkin, and C. Uhler. Simple, fast, and flexible framework for matrix completion with infinite width neural networks. *Proceedings of the National Academy of Sciences*, 119(16):e2115064119, 2022.
- [70] A. Ramesh, M. Pavlov, G. Goh, S. Gray, C. Voss, A. Radford, M. Chen, and I. Sutskever. Zero-shot text-to-image generation. In *International Conference on Machine Learning*, 2021.
- [71] D. A. Roberts, S. Yaida, and B. Hanin. *The Principles of Deep Learning Theory: An Effective Theory Approach to Understanding Neural Networks*. Cambridge University Press, 2022.
- [72] S. T. Roweis and L. K. Saul. Nonlinear dimensionality reduction by locally linear embedding. *Science*, 290(5500):2323–2326, 2000.
- [73] I. Rubachev, A. Alekberov, Y. Gorishniy, and A. Babenko. Revisiting pretraining objectives for tabular deep learning. *arXiv preprint arXiv:2207.03208*, 2022.
- [74] M. Sahraee-Ardakan, M. Emami, P. Pandit, S. Rangan, and A. K. Fletcher. Kernel methods and multi-layer perceptrons learn linear models in high dimensions. *arXiv preprint arXiv:2201.08082*, 2022.
- [75] J. Schmidt-Hieber. Nonparametric regression using deep neural networks with relu activation function. *The Annals of Statistics*, 48(4):1875–1897, 2020.
- [76] S. Schoenholz, J. Gilmer, S. Ganguli, and J. Sohl-Dickstein. Deep information propagation. *arXiv preprint arXiv:1611.01232*, 2016.
- [77] B. Schölkopf and A. J. Smola. *Learning with Kernels: Support Vector Machines, Regularization, Optimization, and Beyond*. MIT Press, 2002.
- [78] R. R. Selvaraju, M. Cogswell, A. Das, R. Vedantam, D. Parikh, and D. Batra. Grad-cam: Visual explanations from deep networks via gradient-based localization. In *International Conference on Computer Vision*, pages 618–626, 2017.
- [79] H. Shah, K. Tamuly, A. Raghunathan, P. Jain, and P. Netrapalli. The pitfalls of simplicity bias in neural networks. *Advances in Neural Information Processing Systems*, 33:9573–9585, 2020.
- [80] Z. Shi, J. Wei, and Y. Lian. A theoretical analysis on feature learning in neural networks: Emergence from inputs and advantage over fixed features. In *International Conference on Learning Representations*, 2022.
- [81] A. Shrikumar, P. Greenside, and A. Kundaje. Learning important features through propagating activation differences. In *International Conference on Machine Learning*, 2017.
- [82] S. Singla and S. Feizi. Salient ImageNet: How to discover spurious features in deep learning? In *International Conference on Learning Representations*, 2022.

- [83] A. Sinha and J. C. Duchi. Learning kernels with random features. *Advances in Neural Information Processing Systems*, 29, 2016.
- [84] L. Sirovich and M. Kirby. Low-dimensional procedure for the characterization of human faces. *JOSA A*, 4(3):519–524, 1987.
- [85] G. Somepalli, M. Goldblum, A. Schwarzschild, C. B. Bruss, and T. Goldstein. Saint: Improved neural networks for tabular data via row attention and contrastive pre-training. *arXiv preprint arXiv:2106.01342*, 2021.
- [86] C. Szegedy, W. Zaremba, I. Sutskever, J. Bruna, D. Erhan, I. Goodfellow, and R. Fergus. Intriguing properties of neural networks. In *International Conference on Learning Representations*, 2014.
- [87] R. Tibshirani. Regression shrinkage and selection via the lasso. *Journal of the Royal Statistical Society: Series B (Methodological)*, 58(1):267–288, 1996.
- [88] S. Trivedi, J. Wang, S. Kpotufe, and G. Shakhnarovich. A consistent estimator of the expected gradient outerproduct. In *UAI*, pages 819–828, 2014.
- [89] K. Tunyasuvunakool, J. Adler, Z. Wu, T. Green, M. Zielinski, A. Židek, A. Bridgland, A. Cowie, C. Meyer, A. Laydon, S. Velankar, G. Kleywegt, A. Bateman, R. Evans, A. Pritzel, M. Figurnov, O. Ronneberger, R. Bates, S. Kohl, and D. Hassabis. Highly accurate protein structure prediction for the human proteome. *Nature*, 596:1–9, 2021.
- [90] M. A. Turk and A. P. Pentland. Face recognition using eigenfaces. In *Conference on Computer Vision and Pattern Recognition*, pages 586–587. IEEE Computer Society, 1991.
- [91] G. Valle-Perez, C. Q. Camargo, and A. A. Louis. Deep learning generalizes because the parameter-function map is biased towards simple functions. In *International Conference on Learning Representations*, 2019.
- [92] S. Van Der Walt, S. C. Colbert, and G. Varoquaux. The numpy array: a structure for efficient numerical computation. *Computing in Science & Engineering*, 13(2):22, 2011.
- [93] N. Vyas, Y. Bansal, and P. Nakkiran. Limitations of the ntk for understanding generalization in deep learning. *arXiv preprint arXiv:2206.10012*, 2022.
- [94] G. Wahba. *Spline models for observational data*. SIAM, 1990.
- [95] T. Wang, D. Zhao, and S. Tian. An overview of kernel alignment and its applications. *Artificial Intelligence Review*, 43:179–192, 2015.
- [96] L. Xiao, Y. Bahri, J. Sohl-Dickstein, S. Schoenholz, and J. Pennington. Dynamical isometry and a mean field theory of cnns: How to train 10,000-layer vanilla convolutional neural networks. In *International Conference on Machine Learning*, pages 5393–5402. PMLR, 2018.
- [97] L. Xiao, J. Pennington, and S. Schoenholz. Disentangling trainability and generalization in deep learning. In *International Conference on Machine Learning*, 2019.
- [98] G. Yang. Scaling limits of wide neural networks with weight sharing: Gaussian process behavior, gradient independence, and neural tangent kernel derivation. *arXiv preprint arXiv:1902.04760*, 2019.
- [99] G. Yang and E. J. Hu. Tensor Programs IV: Feature learning in infinite-width neural networks. In *International Conference on Machine Learning*, 2021.
- [100] G. Yang and S. Schoenholz. Mean field residual networks: On the edge of chaos. *Advances in neural information processing systems*, 30, 2017.
- [101] G. Yang and S. Schoenholz. Deep mean field theory: Layerwise variance and width variation as methods to control gradient explosion. 2018.

- [102] M. D. Zeiler and R. Fergus. Visualizing and understanding convolutional networks. In *European Conference on Computer Vision*, pages 818–833. Springer, 2014.
- [103] C. Zhang, S. Bengio, M. Hardt, B. Recht, and O. Vinyals. Understanding deep learning requires rethinking generalization. In *International Conference on Learning Representations*, 2017.
- [104] C.-H. Zhang and S. S. Zhang. Confidence intervals for low dimensional parameters in high dimensional linear models. *Journal of the Royal Statistical Society: Series B (Statistical Methodology)*, 76(1):217–242, 2014.
- [105] K. Zhang and Y.-X. Wang. Deep learning meets nonparametric regression: Are weight-decayed dnns locally adaptive? *arXiv preprint arXiv:2204.09664*, 2022.
- [106] L. Zhu, C. Liu, and M. Belkin. Transition to linearity of general neural networks with directed acyclic graph architecture. In *Advances in Neural Information Processing Systems*, 2022.
- [107] L. Zhu, C. Liu, A. Radhakrishnan, and M. Belkin. Quadratic models for understanding neural network dynamics. *arXiv preprint arXiv:2205.11787*, 2022.

A Theoretical evidence connecting feature learning to expected gradient outer product

An outline of our theoretical results is provided in Table 1. Below, we provide proofs for our theoretical results. In our proofs, for a matrix $A_\alpha \in \mathbb{R}^{c \times d}$, we denote its p -th row by $A_{\alpha,p}$. For a vector $v \in \mathbb{R}^d$, we denote its i -th element by $v(i)$. We drop the subscript t if it is irrelevant (e.g., fixed) in an expression.

We begin by proving that the neural feature matrix equals the expected gradient outer product provided the outer layer weights are sampled independently of the first layer weights. One such way to achieve this condition in practice is to re-sample the outer weights after training.

Proposition 3 (Shallow, non-linear network). *Consider a fully connected network g with 1 hidden layer, and activation function $\phi(z) = \max\{0, z\}$. Let $\{x_i, y_i\}_{i=1}^n \subset \mathbb{R}^d \times \mathbb{R}$. Let W_1 be fixed and arbitrary (e.g. from training a neural network). Suppose we sample $a_{k'}$ in an i.i.d. manner so that $\mathbb{E}[a_{k'}^2] = 1$ and $\mathbb{E}[a_{k'}] = 0$, and $a_{k'}$. Then, where $x \sim \mathcal{N}(0, I_d)$, we have the following relation,*

$$\frac{1}{k} W_1^\top W_1 = \mathbb{E}_{a,x} \left[\nabla_x g(x) \nabla_x g(x)^\top \right] .$$

The proof of this proposition follows from that of Theorem 1 presented below.

Proof of Theorem 1. We consider the right hand side of the desired equation. The gradient with respect to the input is given by

$$\begin{aligned} \nabla_x g(x) &= \frac{c_\phi^L}{\prod_{\ell=1}^L k_\ell} \sum_{k'_L} \sum_{k'_{L-1}} \cdots \sum_{k'_1} a_{k'_L} \phi'(W_{L,k'_L}^\top \phi_{L-1}(z)) \\ &\quad \cdot W_{L,k'_L}(k'_{L-1}) \phi'(W_{L-1,k'_{L-1}}^\top \phi_{L-2}(x)) \cdots W_{3,k'_3}(k'_2) \cdot \phi'(W_{2,k'_2}^\top \phi_1(x)) \\ &\quad \cdot W_{2,k'_2}(k'_1) \phi'(W_{1,k'_1}^\top x) \cdot W_{1,k'_1} . \end{aligned}$$

Then,

$$\begin{aligned}
\nabla_x g(x) \nabla_x g(x)^\top &= \frac{c_\phi^L}{\prod_{\ell=1}^L k_\ell} \\
&\cdot \sum_{k'_L, k''_L} \sum_{k'_{L-1}, k''_{L-1}} \dots \sum_{k'_1, k''_1} \phi' \left(W_{L, k'_L}^\top \phi_{L-1}(x) \right) \dots \phi' \left(W_{2, k'_2}^\top \phi(W_1 x) \right) \phi' \left((W_{1, k'_1})^\top x \right) \\
&\cdot \phi' \left(W_{L, k''_L}^\top \phi_{L-1}(x) \right) \dots \phi' \left(W_{2, k''_2}^\top \phi(W_1 x) \right) \phi' \left((W_{1, k''_1})^\top x \right) \\
&\cdot a_{k'_L} W_{L, k'_L}(k'_{L-1}) \dots W_{3, k'_3}(k'_2) W_{2, k'_2}(k'_1) \\
&\cdot a_{k''_L} W_{L, k''_L}(k''_{L-1}) \dots W_{3, k''_3}(k''_2) W_{2, k''_2}(k''_1) \\
&\cdot W_{1, k'_1} W_{1, k''_1}^\top.
\end{aligned}$$

By the gradient independence ansatz, we can generate new samples $\widetilde{W}_L, \dots, \widetilde{W}_2$,

$$\begin{aligned}
\lim_{k_2, \dots, k_L \rightarrow \infty} \mathbb{E}_a \nabla_x g(x) \nabla_x g(x)^\top &= \lim_{k_2, \dots, k_L \rightarrow \infty} \mathbb{E}_a \frac{c_\phi^L}{\prod_{\ell=1}^L k_\ell} \sum_{k'_L, k''_L} \sum_{k'_{L-1}, k''_{L-1}} \dots \sum_{k'_1, k''_1} \\
&\cdot \phi' \left(W_{L, k'_L}^\top \phi_{L-1}(x) \right) \dots \phi' \left(W_{2, k'_2}^\top \phi(W_1 x) \right) \phi' \left((W_{1, k'_1})^\top x \right) \\
&\cdot \phi' \left(W_{L, k''_L}^\top \phi_{L-1}(x) \right) \dots \phi' \left(W_{2, k''_2}^\top \phi(W_1 x) \right) \phi' \left((W_{1, k''_1})^\top x \right) \\
&\cdot a_{k'_L} \widetilde{W}_{L, k'_L}(k'_{L-1}) \dots \widetilde{W}_{3, k'_3}(k'_2) \widetilde{W}_{2, k'_2}(k'_1) \\
&\cdot a_{k''_L} \widetilde{W}_{L, k''_L}(k''_{L-1}) \dots \widetilde{W}_{3, k''_3}(k''_2) \widetilde{W}_{2, k''_2}(k''_1) \\
&\cdot W_{1, k'_1} W_{1, k''_1}^\top.
\end{aligned}$$

Pulling factors outside of the limit,

$$\begin{aligned}
&= \lim_{k_2, \dots, k_{L-1} \rightarrow \infty} \frac{c_\phi^L}{\prod_{\ell=1}^{L-1} k_\ell} \\
&\lim_{k_L \rightarrow \infty} \frac{1}{k_L} \sum_{k'_L} \left(\phi' \left(W_{L, k'_L}^\top \phi_{L-1}(x) \right) \right)^2 \\
&\sum_{k'_{L-1}, k''_{L-1}} \widetilde{W}_{L, k'_L}(k'_{L-1}) \widetilde{W}_{L, k'_L}(k'_{L-1}) \\
&\cdot \sum_{k'_{L-2}, k''_{L-2}} \dots \sum_{k'_1, k''_1} \phi' \left(W_{L-1, k'_{L-1}}^\top \phi_{L-2}(x) \right) \dots \phi' \left(W_{2, k'_2}^\top \phi(W_1 x) \right) \phi' \left((W_{1, k'_1})^\top x \right) \\
&\cdot \phi' \left(W_{L-1, k''_{L-1}}^\top \phi_{L-2}(x) \right) \dots \phi' \left(W_{2, k''_2}^\top \phi(W_1 x) \right) \phi' \left((W_{1, k''_1})^\top x \right) \\
&\cdot \widetilde{W}_{L-1, k'_{L-1}}(k'_{L-2}) \dots \widetilde{W}_{3, k'_3}(k'_2) \widetilde{W}_{2, k'_2}(k'_1) \\
&\cdot \widetilde{W}_{L-1, k''_{L-1}}(k''_{L-2}) \dots \widetilde{W}_{3, k''_3}(k''_2) \widetilde{W}_{2, k''_2}(k''_1) \\
&\cdot W_{1, k'_1} W_{1, k''_1}^\top.
\end{aligned}$$

Note that by re-sampling, $\left(\phi' \left(W_{L, k'_L}^\top \phi_{L-1}(x) \right) \right)^2$ is independent of the remaining terms, and so we can

apply the law of large numbers as $k_L \rightarrow \infty$ and split the expectation as follows.

$$\begin{aligned}
\lim_{k_2, \dots, k_L \rightarrow \infty} \mathbb{E}_a \nabla_x g(x) \nabla_x g(x)^\top &= \lim_{k_2, \dots, k_{L-1} \rightarrow \infty} \frac{c_\phi^L}{\prod_{\ell=1}^{L-1} k_\ell} \\
&\mathbb{E}_{k'_L} \left[\left(\phi' \left(W_{L, k'_L}^\top \phi_{L-1}(x) \right) \right)^2 \right] \\
&\mathbb{E}_{k'_L} \left[\sum_{k'_{L-1}, k''_{L-1}} \widetilde{W}_{L, k'_L}(k'_{L-1}) \widetilde{W}_{L, k'_L}(k'_{L-1}) \right. \\
&\quad \cdot \sum_{k'_{L-2}, k''_{L-2}} \dots \sum_{k'_1, k''_1} \phi' \left(W_{L-1, k'_{L-1}}^\top \phi_{L-2}(x) \right) \dots \phi' \left(W_{2, k'_2}^\top \phi(W_1 x) \right) \phi'((W_{1, k'_1})^\top x) \\
&\quad \cdot \phi' \left(W_{L-1, k''_{L-1}}^\top \phi_{L-2}(x) \right) \dots \phi' \left(W_{2, k''_2}^\top \phi(W_1 x) \right) \phi'((W_{1, k''_1})^\top x) \\
&\quad \cdot \widetilde{W}_{L-1, k'_{L-1}}(k'_{L-2}) \dots \widetilde{W}_{3, k'_3}(k'_2) \widetilde{W}_{2, k'_2}(k'_1) \\
&\quad \cdot \widetilde{W}_{L-1, k''_{L-1}}(k''_{L-2}) \dots \widetilde{W}_{3, k''_3}(k''_2) \widetilde{W}_{2, k''_2}(k''_1) \\
&\quad \left. \cdot W_{1, k'_1} W_{1, k''_1}^\top \right].
\end{aligned}$$

Evaluating the expectations above, we conclude:

$$\begin{aligned}
\lim_{k_2, \dots, k_L \rightarrow \infty} \mathbb{E}_a \nabla_x g(x) \nabla_x g(x)^\top &= \lim_{k_2, \dots, k_{L-1} \rightarrow \infty} \frac{c_\phi^{L-1}}{\prod_{\ell=1}^{L-1} k_\ell} \\
&\cdot \sum_{k'_{L-1}} \sum_{k'_{L-2}, k''_{L-2}} \dots \sum_{k'_1, k''_1} \phi' \left(W_{L-1, k'_{L-1}}^\top \phi_{L-2}(x) \right) \dots \phi' \left(W_{2, k'_2}^\top \phi(W_1 x) \right) \phi'((W_{1, k'_1})^\top x) \\
&\cdot \phi' \left(W_{L-1, k'_{L-1}}^\top \phi_{L-2}(x) \right) \dots \phi' \left(W_{2, k''_2}^\top \phi(W_1 x) \right) \phi'((W_{1, k''_1})^\top x) \\
&\cdot \widetilde{W}_{L-1, k'_{L-1}}(k'_{L-2}) \dots \widetilde{W}_{3, k'_3}(k'_2) \widetilde{W}_{2, k'_2}(k'_1) \\
&\cdot \widetilde{W}_{L-1, k'_{L-1}}(k''_{L-2}) \dots \widetilde{W}_{3, k''_3}(k''_2) \widetilde{W}_{2, k''_2}(k''_1) \\
&\cdot W_{1, k'_1} W_{1, k''_1}^\top.
\end{aligned}$$

Recursively applying this procedure yields

$$\lim_{k_2, \dots, k_L \rightarrow \infty} \mathbb{E}_a \nabla_x g(x) \nabla_x g(x)^\top = \frac{c_\phi}{k_1} \sum_{k'_1} \phi'((W_{1, k'_1})^\top x)^2 W_{1, k'_1} W_{1, k'_1}^\top.$$

Taking the expectation with respect to x ,

$$\mathbb{E}_x \left[\lim_{k_2, \dots, k_L \rightarrow \infty} \mathbb{E}_a \nabla_x g(x) \nabla_x g(x)^\top \right] = \frac{1}{k_1} \sum_{k'_1} W_{1, k'_1} W_{1, k'_1}^\top.$$

□

We next analyze feature learning in two layer linear neural networks where only the first layer is trained without using the gradient independence ansatz.

Proposition 4 (Linear, Full GD). *Let $f : \mathbb{R}^d \rightarrow \mathbb{R}$ denote a two layer neural network of the form*

$$f(x) = A \frac{1}{\sqrt{k}} Bx;$$

where $A \in \mathbb{R}^{1 \times k}$, $B \in \mathbb{R}^{k \times d}$. Consider the case where only B is trainable. Let $B^{(t)}$ and $f^{(t)}$ denote updated weights after t steps of gradient descent on the dataset $(X, y) \in \mathbb{R}^{d \times n} \times \mathbb{R}^{1 \times n}$ with constant learning rate $\eta > 0$. If $\{A_i^{(0)}\}_{i=1}^k$ are i.i.d. random variables $\mathbb{E}[A_i^2] = 1$ and $B^{(0)} = \mathbf{0}$,

$$\lim_{k \rightarrow \infty} B^{(t)\top} B^{(t)} = \lim_{k \rightarrow \infty} \nabla f^{(t)} \nabla f^{(t)\top} ;$$

where $\nabla f^{(t)}$ is the gradient of $f^{(t)}$.¹⁵

Proof of Proposition 4. The gradient descent updates proceed as follows:

$$B^{(t+1)} = B^{(t)} + \frac{\eta}{\sqrt{k}} A^{(0)\top} \left(y - A^{(0)} \frac{1}{\sqrt{k}} B^{(t)} X \right) X^\top .$$

We provide a proof by induction. We begin with the base case with $t = 1$. The base case follows from the fact that $\lim_{k \rightarrow \infty} \frac{1}{k} A^{(0)} A^{(0)\top} = 1$ and $B^{(1)} = \frac{\eta}{\sqrt{k}} A^{(0)\top} y X^\top$ and thus,

$$\begin{aligned} \lim_{k \rightarrow \infty} B^{(1)\top} B^{(1)} &= \lim_{k \rightarrow \infty} \frac{\eta^2}{k} X y^\top A^{(0)} A^{(0)\top} y X^\top = \eta^2 X y^\top y X^\top ; \\ \lim_{k \rightarrow \infty} \nabla f_1 \nabla f_1^\top &= \lim_{k \rightarrow \infty} B^{(1)\top} A^{(0)\top} \frac{1}{k} A^{(0)} B^{(1)} \\ &= \lim_{k \rightarrow \infty} \eta^2 X y^\top \left(A^{(0)} \frac{1}{k} A^{(0)\top} \right) \left(A^{(0)} \frac{1}{k} A^{(0)\top} \right) y X^\top = \eta^2 X y^\top y X^\top . \end{aligned}$$

Thus, we now assume the inductive hypothesis that

$$\lim_{k \rightarrow \infty} B^{(t)\top} B^{(t)} = \lim_{k \rightarrow \infty} \nabla f^{(t)} \nabla f^{(t)\top}$$

and analyze the case for timestep $t + 1$. We first have:

$$\begin{aligned} B^{(t+1)\top} B^{(t+1)} &= \left[B^{(t)} + \frac{\eta}{\sqrt{k}} A^{(0)\top} \left(y - A^{(0)} \frac{1}{\sqrt{k}} B^{(t)} X \right) X^\top \right]^\top \left[B^{(t)} + \frac{\eta}{\sqrt{k}} A^{(0)\top} \left(y - A^{(0)} \frac{1}{\sqrt{k}} B^{(t)} X \right) X^\top \right] \\ &= B^{(t)\top} B^{(t)} + B^{(t)\top} \frac{\eta}{\sqrt{k}} A^{(0)\top} y X^\top - B^{(t)\top} \frac{\eta}{k} A^{(0)\top} A^{(0)} B^{(t)} X X^\top \\ &\quad + \frac{\eta}{\sqrt{k}} X y^\top A^{(0)} B^{(t)} + \frac{\eta^2}{k} X y^\top A^{(0)} A^{(0)\top} y X^\top - \frac{\eta^2}{k} X y^\top A^{(0)} A^{(0)\top} A^{(0)} \frac{1}{\sqrt{k}} B^{(t)} X X^\top \\ &\quad - \frac{\eta}{k} X X^\top B^{(t)\top} A^{(0)\top} A^{(0)} B^{(t)} - \frac{\eta^2}{k} X X^\top B^{(t)\top} \frac{1}{\sqrt{k}} A^{(0)\top} A^{(0)} A^{(0)\top} y X^\top \\ &\quad + \frac{\eta^2}{k^2} X X^\top B^{(t)\top} A^{(0)\top} A^{(0)} A^{(0)\top} A^{(0)} B^{(t)} X X^\top . \end{aligned}$$

To simplify notation, we let

$$Z = \lim_{k \rightarrow \infty} A^{(0)} \frac{1}{\sqrt{k}} B^{(t)} \quad ; \quad M = \lim_{k \rightarrow \infty} B^{(t)\top} B^{(t)} ,$$

noting that for $x \in \mathbb{R}^d$, Zx converges in distribution to a standard normal random variable by the central limit theorem. Taking the limit as $k \rightarrow \infty$, applying the inductive hypothesis and the fact that $\lim_{k \rightarrow \infty} \frac{1}{k} A^{(0)} A^{(0)\top} = 1$, we reduce the above to

$$\begin{aligned} \lim_{k \rightarrow \infty} B^{(t+1)\top} B^{(t+1)} &= M + \eta Z^\top y X^\top - \eta M X X^\top \\ &\quad + \eta X y^\top Z + \eta^2 X y^\top y X^\top - \eta^2 X y^\top Z X X^\top \\ &\quad - \eta X X^\top M - \eta^2 X X^\top Z^\top y X^\top + \eta^2 X X^\top M X X^\top . \end{aligned}$$

¹⁵Note that since $f^{(t)}$ is linear, the gradient is constant.

We will now show that $\lim_{k \rightarrow \infty} \nabla f^{(t+1)} \nabla f^{(t+1)^\top}$ is of the same form. Namely, we have

$$\begin{aligned}
\nabla f^{(t+1)} \nabla f^{(t+1)^\top} &= B^{(t+1)^\top} A^{(0)\top} \frac{1}{k} A^{(0)} B^{(t+1)} \\
&= B^{(t)^\top} A^{(0)\top} \frac{1}{k} A^{(0)} B^{(t)} + B^{(t)^\top} A^{(0)\top} \frac{1}{k} A^{(0)} \frac{\eta}{\sqrt{k}} A^{(0)\top} y X^\top \\
&\quad - B^{(t)^\top} A^{(0)\top} \frac{1}{k} A^{(0)} \frac{\eta}{k} A^{(0)\top} A^{(0)} B^{(t)} X X^\top \\
&\quad + \frac{\eta}{\sqrt{k}} X y^\top A^{(0)} A^{(0)\top} \frac{1}{k} A^{(0)} B^{(t)} + \frac{\eta^2}{k} X y^\top A^{(0)} A^{(0)\top} \frac{1}{k} A^{(0)} A^{(0)\top} y X^\top \\
&\quad - \frac{\eta^2}{k} X y^\top A^{(0)} A^{(0)\top} \frac{1}{k} A^{(0)} A^{(0)\top} A^{(0)} \frac{1}{\sqrt{k}} B^{(t)} X X^\top \\
&\quad - \frac{\eta}{\sqrt{k}} X X^\top B^{(t)^\top} A^{(0)\top} A^{(0)} A^{(0)\top} \frac{1}{k} A^{(0)} B^{(t)} \\
&\quad - \frac{\eta^2}{k} X X^\top B^{(t)^\top} \frac{1}{\sqrt{k}} A^{(0)\top} A^{(0)} A^{(0)\top} \frac{1}{k} A^{(0)} A^{(0)\top} y X^\top \\
&\quad + \frac{\eta^2}{k^2} X X^\top B^{(t)^\top} A^{(0)\top} A^{(0)} A^{(0)\top} \frac{1}{k} A^{(0)} A^{(0)\top} A^{(0)} B^{(t)} X X^\top.
\end{aligned}$$

Now taking the limit as $k \rightarrow \infty$, we reduce the above to

$$\begin{aligned}
\lim_{k \rightarrow \infty} \nabla f^{(t+1)} \nabla f^{(t+1)^\top} &= M + \eta Z^\top y X^\top - \eta M X X^\top \\
&\quad + \eta X y^\top Z + \eta^2 X y^\top y X^\top - \eta^2 X y^\top Z X X^\top \\
&\quad - \eta X X^\top M - \eta^2 X X^\top Z^\top y X^\top + \eta^2 X X^\top M X X^\top.
\end{aligned}$$

Hence, we conclude

$$\lim_{k \rightarrow \infty} B^{(t+1)^\top} B^{(t+1)} = \lim_{k \rightarrow \infty} \nabla f^{(t+1)} \nabla f^{(t+1)^\top},$$

which completes the proof by induction. \square

In the following proposition, we extend the previous analysis to the case of two layer linear neural networks where both layers are trained for two steps of gradient descent. Again, we no longer use the gradient independence ansatz.

Proposition 5. *Let $f : \mathbb{R}^d \rightarrow \mathbb{R}$ denote a two layer neural network of the form*

$$f(x) = A \frac{1}{\sqrt{k}} B x;$$

where $A \in \mathbb{R}^{1 \times k}$, $B \in \mathbb{R}^{k \times d}$. Let $A^{(t)}$, $B^{(t)}$ and $f^{(t)}$ denote updated weights after t steps of gradient descent on the dataset $(X, y) \in \mathbb{R}^{d \times n} \times \mathbb{R}^{1 \times n}$ with constant learning rate $\eta > 0$. If $\{A_i^{(0)}\}_{i=1}^k$ are i.i.d. random variables $\mathbb{E}[A_i^{(0)^2}] = 1$ and $B^{(0)} = \mathbf{0}$,

$$\lim_{k \rightarrow \infty} B^{(2)^\top} B^{(2)} = \lim_{k \rightarrow \infty} \nabla f^{(2)} \nabla f^{(2)^\top};$$

where $\nabla f^{(2)}$ is the gradient of $f^{(2)}$.

Proof. We prove the statement directly. The gradient descent updates proceed as follows:

$$\begin{aligned}
A^{(t+1)} &= A^{(t)} + \frac{\eta}{\sqrt{k}} \left(y - A^{(t)} \frac{1}{\sqrt{k}} B^{(t)} X \right) X^\top B^{(t)^\top}, \\
B^{(t+1)} &= B^{(t)} + \frac{\eta}{\sqrt{k}} A^{(t)^\top} \left(y - A^{(t)} \frac{1}{\sqrt{k}} B^{(t)} X \right) X^\top.
\end{aligned}$$

Thus, after 1 step of gradient descent, we have

$$A^{(1)} = A^{(0)} \quad ; \quad B^{(1)} = \frac{\eta}{\sqrt{k}} A^{(0)\top} y X^\top.$$

From the proof of Proposition 4, we have that

$$\lim_{k \rightarrow \infty} B^{(1)\top} B^{(1)} = \lim_{k \rightarrow \infty} B^{(1)\top} \frac{1}{k} A^{(0)\top} A^{(0)} B^{(1)},$$

and so, we define the matrix M to be:

$$M := \lim_{k \rightarrow \infty} B^{(1)\top} B^{(1)}.$$

Next, after 2 steps of gradient descent, we have:

$$\begin{aligned} A^{(2)} &= A^{(1)} + \frac{\eta}{\sqrt{k}} \left(y - A^{(1)} \frac{1}{\sqrt{k}} B^{(1)} X \right) X^\top B^{(1)\top} \\ &= A^{(0)} + \frac{\eta}{\sqrt{k}} y X^\top B^{(1)\top} - \frac{\eta}{k} A^{(0)} B^{(1)} X X^\top B^{(1)\top} \\ &= A^{(0)} + \frac{\eta^2}{k} y X^\top X y^\top A^{(0)} - \frac{\eta^3}{k^2} A^{(0)} A^{(0)\top} y X^\top X X^\top X y^\top A^{(0)}; \end{aligned}$$

and

$$\begin{aligned} B^{(2)} &= B^{(1)} + \frac{\eta}{\sqrt{k}} A^{(1)\top} \left(y - A^{(1)} \frac{1}{\sqrt{k}} B^{(1)} X \right) X^\top \\ &= \frac{2\eta}{\sqrt{k}} A^{(0)\top} y X^\top - \frac{\eta}{k} A^{(0)\top} A^{(0)} B^{(1)} X X^\top \\ &= \frac{2\eta}{\sqrt{k}} B^{(1)} - \frac{\eta}{k} A^{(0)\top} A^{(0)} B^{(1)} X X^\top. \end{aligned}$$

Thus, we simplify $B^{(2)\top} B^{(2)}$ as follows:

$$\begin{aligned} B^{(2)\top} B^{(2)} &= \frac{4\eta^2}{k} B^{(1)\top} B^{(1)} - \frac{2\eta^2}{k\sqrt{k}} B^{(1)\top} A^{(0)\top} A^{(0)} B^{(1)} X X^\top \\ &\quad - \frac{2\eta^2}{k\sqrt{k}} X X^\top B^{(1)\top} A^{(0)\top} A^{(0)} B^{(1)} + \frac{\eta^2}{k^2} X X^\top B^{(1)\top} A^{(0)\top} A^{(0)} A^{(0)\top} A^{(0)} B^{(1)} X X^\top. \end{aligned}$$

Taking the limit as $k \rightarrow \infty$, we simplify the above expression to

$$\lim_{k \rightarrow \infty} B^{(2)\top} B^{(2)} = 4\eta^2 M + \eta^2 X X^\top M X X^\top.$$

A key observation is that as $k \rightarrow \infty$, the $O\left(\frac{1}{k}\right)$ and $O\left(\frac{1}{k^2}\right)$ terms in $A^{(2)}$ will vanish in the evaluation of $\lim_{k \rightarrow \infty} \nabla f^{(2)} \nabla f^{(2)\top}$ since the gradient also contains an extra $\frac{1}{\sqrt{k}}$ term from f . Hence only the $O(1)$ terms given by $A^{(0)}$ will remain in the evaluation of $\lim_{k \rightarrow \infty} \nabla f^{(2)} \nabla f^{(2)\top}$. Using this observation, we have:

$$\lim_{k \rightarrow \infty} \nabla f^{(2)} \nabla f^{(2)\top} = \lim_{k \rightarrow \infty} B^{(2)\top} \frac{1}{k} A^{(2)\top} A^{(2)} B^{(2)} = \lim_{k \rightarrow \infty} B^{(2)\top} \frac{1}{k} A^{(0)\top} A^{(0)} B^{(2)},$$

which by the expansion of $B^{(2)\top} B^{(2)}$ and the proof of Proposition 4, is equivalent to $4\eta^2 M + \eta^2 X X^\top M X X^\top$. \square

B Background on Kernel Ridge Regression

We here provide a brief review of kernel ridge regression [77]. Given a dataset $\{(x_i, y_i)\}_{i=1}^n \subset \mathbb{R}^d \times \mathbb{R}$ and a Hilbert space, \mathcal{H} , kernel ridge regression constructs an non-parametric estimator given by

$$\hat{f}_{n,\lambda} = \operatorname{argmin}_{f \in \mathcal{H}} \sum_{i=1}^n (f(x_i) - y_i)^2 + \lambda \|f\|_{\mathcal{H}}^2; \quad (2)$$

where $\lambda \geq 0$ is referred to as the ridge regularization parameter. Note this is an infinite dimensional optimization problem in a Reproducing Kernel Hilbert Space, \mathcal{H} , corresponding to a positive semi-definite kernel function K . By virtue of the Representer theorem [94], this problem has a unique solution in the span of the data given by

$$\hat{f}_{n,\lambda} = \sum_{i=1}^n \hat{\alpha}_i K(x, x_i) \quad \text{where} \quad \hat{\alpha} = y(K(X, X) + \lambda I_n)^{-1}; \quad (3)$$

where $K(X, X)_{ij} = K(x_i, x_j)$ and $y \in \mathbb{R}^{1 \times n}$. Naively, this involves solving a $n \times n$ linear system, which can be typically solved in closed form for $n \leq 100,000$. For $n > 100,000$, we apply the EigenPro solver [55] to approximately solve kernel regression via early-stopped, preconditioned-SGD that can run on the GPU. For $\lambda \rightarrow 0^+$, we recover the pseudo-inverse solution $\hat{\alpha} = yK(X, X)^\dagger$. For multi-class and multi-variate problems, y_i are vector valued and we consider each class/target variable as a separate problem.

C Sample complexity improvement with RFMs

We demonstrate that one can obtain a provable improvement in sample complexity using RFM (and applying the expected gradient outer product transformation in general) in the case that the target function depends on only a few relevant directions of the input.

Definition 2 (Rank- r function). *A function $f : \mathbb{R}^d \rightarrow \mathcal{Y}$ has **rank** r if there exists a matrix $U \in \mathbb{R}^{r \times d}$ such that $f(x) = g(Ux)$ for some other function $g : \mathbb{R}^r \rightarrow \mathcal{Y}$ for all $x \in \mathbb{R}^d$. The matrix U is called the **target subspace** and its **span** is the span of its rows.*

Proof of Proposition 2. The gradient of the target function in directions orthogonal to the target subspace U is 0, as the function does not vary in these directions. Thus, $\nabla f^*(x)$ is in the span of U . Hence, for any $x' \in \mathbb{R}^d$, as

$$Mx' = \mathbb{E}_{x \in X_N} [\nabla f^*(x) \nabla f^*(x)^T x'] ,$$

we have that Mx' is also in the span of U . Therefore, the transformed data $M^{\frac{1}{2}}X$ lies in an r -dimensional subspace and have an equivalent representation in an r -dimensional coordinate space. In other words, for all $i, j \in [d]$, there exists $\alpha_i, \alpha_j \in \mathbb{R}^r$ such that $\|x_i - x_j\| = \|\alpha_i - \alpha_j\|$. Further, the degree of the target function does not change under linear transformation or rotation. The final bound follows from the generalization error bound of linear regression for kernel ridge regression with a polynomial kernel of degree r . \square

D Dataset and Experimental Details

Below, we provide a description of all datasets, models, and training methodology considered in this work.

Experiments with RFMs and fully connected networks on CelebA. For all binary classification tasks on CelebA in this work, we normalize all images to be on the unit sphere. We train 2-hidden layer ReLU networks with 1024 hidden units per layer using stochastic gradient descent (SGD) for 500 epochs with a learning rate of 0.1 and a mini-batch size of 128. We train using the mean squared error (MSE) with one-hot labels for each of the classes. Accuracy is reported as the argmax across classes. We train RFMs for 1 iteration, use a ridge regularization term of 10^{-3} , and average the gradient outer product of at most 20000

examples. All RFMs use Laplace kernels as the base kernel and use a bandwidth parameter of $L = 10$. We solve kernel ridge regression exactly via the solve function in numpy [92].

For all classification tasks, we split available training data into 80% training and 20% validation for hyper-parameter selection. We report accuracy on a held out test set provided by PyTorch [64]. In addition, since there can be large class imbalances in this data, we ensure that the training set and test set are balanced by limiting the number of majority class samples to the same number of minority class samples. Given that these are higher resolution images, we limit the total number of training and validation examples per experiment to 50000 (25000 per class).

For RFM-T experiments in Fig. 6, we retrained a Laplace kernel with bandwidth 10 and ridge regularization of 10^{-3} after thresholding the diagonals of the feature matrix with pixel intensity larger than 0.05 after min-max scaling the feature matrix.

SVHN. We train 2-hidden layer ReLU networks with 1024 hidden units per layer using stochastic gradient descent (SGD) for 500 epochs with a learning rate of 0.05 and a mini-batch size of 100. In Section 6, we train the neural network for 4000 epochs, and extract the neural feature matrix from the step with best validation accuracy. We train using the mean squared error (MSE) with one-hot labels for each of the classes. Accuracy is reported as the argmax across classes. We train RFMs for 5 iterations and average the gradient outer product of at most 20000 examples. We also center gradients during computation of RFMs by subtracting the mean of the gradients before computing the average gradient outer product. RFMs and Laplace kernels used all have a bandwidth parameter of 10. We compare with the NTK of a 2-hidden layer ReLU network. For all kernels, we solve kernel ridge regression with ridge term of 10^{-3} via the solve function in numpy [92]. The test accuracy for RFMs in Fig. 3c is given by training a 1-hidden layer NTK with ridge regularization of 10^{-2} on the feature matrix selected from the last iteration of training, which resulted in the best validation accuracy.

We split available training data into 80% training and 20% validation for hyper-parameter selection. We report accuracy on a held out test set provided by PyTorch [64].

Low rank polynomials. We consider the low rank polynomials from [93] and [22]. We use 1000 examples for training and 10000 samples for testing. Following the setup of [93], we sample training inputs from a Rademacher distribution in 30 dimensions and add random noise (see Fig. 16a). The labels are generated by the product of the first two coordinates of the inputs without noise. We train a 1 hidden layer neural network for 1000 epochs using full batch gradient descent with a learning rate of .1 and initialize the first layer with standard deviation 10^{-3} so as to mitigate the effect of the initialization in the feature matrix. For the experiments in Section 6, we train for only 100 epochs (sufficient for near-interpolation). We train RFMs with no ridge term and set the base kernel function as the Laplace kernel with bandwidth 10. We note the neural network was able to interpolate the training data and achieved a training R^2 of 1.

For the second low rank experiment in Fig. 16d, we sample inputs, x , according to a 10 dimensional isotropic Gaussian distribution and sample a fixed vector, u , on the unit sphere in 10 dimensions. The targets are given by $g(u^T x)$ where $g(z) = \text{He}_2(z) + \text{He}_4(z)$ where He_2, He_4 are the second and fourth probabilist's Hermite polynomials. We train a 1 hidden layer neural network using full batch Adam [42] with a learning rate of 10^{-2} and use the default PyTorch initialization. We train RFMs with no ridge term and set the base kernel function as the Laplace kernel with bandwidth 10. We note the neural network was able to nearly interpolate the training data within 1000 epochs and achieved a training R^2 of 0.971.

121 datasets from [23]. We first describe the experiments for 120 of the 121 datasets with fewer than 130000 examples since we used EigenPro [55] to train kernels on the largest dataset. For all kernel methods (RFMs, Laplace kernel and NTK), we grid search over ridge regularization from the set $\{10, 1, .1, .01, .001\}$. We grid search over 5 iterations for RFMs and used a bandwidth of 10 for all Laplace kernels. For NTK ridge regression experiments, we grid search over NTKs corresponding to ReLU networks with between 1 and 5 hidden layers. For the dataset with 130000 samples, we use EigenPro to train all kernel methods and RFMs. We run EigenPro for at most 50 iterations and select the iteration with best validation accuracy for reporting test accuracy. For small datasets (i.e., those with fewer than 5000 samples), we grid search over updating just the diagonals of M and updating the entire matrix M . Lastly, for all kernel methods

and RFMs, we grid search over normalizing the data to the unit sphere. We note that there is one dataset (balance-scale), which had a data point with norm 0, and so we did not grid search over normalization for this dataset.

Tabular data benchmark from [30]. We used the repository from [30] at <https://github.com/LeoGrin/tabular-benchmark>, modifying the code as needed to incorporate our method. On all datasets, we grid search over 5 iterations of RFM with the Laplace kernel, solving kernel regression in closed form at all steps. This benchmark consists of 20 medium regression datasets (without categorical variables), 3 large regression datasets (without categorical variables), 15 medium classification datasets (without categorical variables), 4 large classification datasets (without categorical variables), 13 medium classification datasets (with categorical variables), 5 large regression datasets (with categorical variables), 7 medium classification datasets (with categorical variables), and 2 large classification datasets (with categorical variables). Following the terminology from [30], “medium” refers to datasets with at most 10000 training examples and “large” refers to those with more than 10000 training examples. In general, we grid-searched over ridge regularization parameters in $\{10^{-4}, 10^{-3}, 10^{-2}, 10^{-1}, 1\}$ with fixed bandwidth $L = 10$. For regression, we centered the labels and scaled their variance to 1. On large regression datasets, we also optimized for bandwidths over $\{1, 5, 10, 15, 20\}$. We searched over two target transformations - the log transform ($\hat{y} = |y| \log(1 + |y|)$) and `sklearn.preprocessing.QuantileTransformer`. In both cases, we inverted the transform before testing. We also searched over data transformations - `sklearn.preprocessing.StandardScaler` and `sklearn.preprocessing.QuantileTransformer`. We also optimized for the use of centering/not centering the gradients in the EGOP computation, and extracting just the diagonal of the EGOP (known as gradient weighting). For non-kernel methods, we compare to the metrics reported in [30]. For classification, we report the average accuracy across the random iterations in each sweep (including random train/val/test splits). For regression, the average R^2 is reported. The reported test score is the average performance of the model with the highest average validation performance.

Grokking. The total number of training and validation samples used is 553 with 500 examples of airplanes and 53 examples of trucks. We use 800 examples per class from the PyTorch test set as test data. We set a small stars of pixels (8 pixels tall, 7 pixels wide) in the upper left corner to yellow (all 1s in the green and red channel) if the image is a truck and all 0s if the image is a plane. We use 80% of the 553 samples for training and 20% for validation. We train a two hidden layer fully connected ReLU network using Adam with a learning rate of 10^{-4} and batch size equal to dataset size. We initialize the weights of the first layer of the ReLU network according to a normal distribution with standard deviation 5×10^{-3} . We train RFMs updating only the diagonals of the feature matrix for three iterations with ridge regularization of 2.5×10^{-3} and using the Laplace kernel as the base kernel function with a bandwidth of 10. We used ridge regularization to slow down training of RFMs to visualize how the feature matrix changes through iteration. We note that without regularization, the RFM gets 100% test accuracy within 1 iteration.

Simplicity bias. For experiment in Fig. 8, we constructed a training set of size 50000 concatenated CIFAR-10 and MNIST digits, and a corresponding test set of 10000 test images. The training and test data were generated from data loaders provided by PyTorch. We used 20% of the training samples were used for validation. We trained a two hidden layer fully connected ReLU network using SGD with a learning rate of 0.1 and a mini-batch size of 100. The RFM was trained for 1 iteration using the Laplace kernel as the base kernel function and ridge regularization of 10^{-3} .

E Description of Metrics for Tabular Benchmarks

Friedman Rank. To compute Friedman rank, we rank classifiers in order of performance (e.g. the top performer gets rank 1) for each dataset and then average the ranks. In the original results of [23], certain classifiers were missing performance values. To compute the Friedman rank, the authors of [23] impute such missing entries via the average classifier performance for this data. We provide code for computing the Friedman rank that replicates the ranks provided in the original work of [23].

Average Accuracy. Average accuracy is just the average over all available accuracies across datasets. In this case, missing accuracies are not imputed for the average and are simply dropped.

Percentage of Maximum Accuracy (PMA). An average over the percentage of the best classifier accuracy achieved by a given model across all datasets.

P90/P95. An average over all datasets for which a classifier achieves within 90%/95% of the accuracy of the best model.

Average Distance to Minimum (ADTM). This metric normalizes for variance in the hardness of different datasets. Let x_{ij} be the performance of method j for dataset i , the ADTM for method j is defined as $\text{ADTM}_j = \text{Avg}_i \left(\frac{x_{ij} - \min_j x_{ij}}{\max_j x_{ij}} \right)$. Note $\text{ADTM} \in [0, 1]$, with 1 indicating a method is the best among all methods in the collection, and 0 indicating a method is the worst.

F Additional experiments on depth

We present the additional experiments on SVHN and low rank polynomials for studying the effect of depth. We observed for SVHN depth did not help accuracy, and, further, a Mahalanobis kernel with the first layer feature matrix is sufficient to exceed the performance of the neural network.

Method	Depth 1 (Acc/MSE)	Depth 2 (Acc/MSE)	Depth 3 (Acc/MSE)	Depth 4 (Acc/MSE)
NN	77.61 % / 0.0538	78.72 % / 0.0476	79.32 % / 0.0413	79.03 % / 0.0405
NTK	73.61 % / 0.0547	73.66 % / 0.0543	73.56 % / 0.0541	73.53 % / 0.0539
NTK + $W_1^T W_1$	82.28 % / 0.0466	79.88 % / 0.0474	79.42 % / 0.0469	78.89 % / 0.0467
Laplace	66.76 % / 0.0549	-	-	-
Laplace + $W_1^T W_1$	79.55 % / 0.0347	79.22 % / 0.0364	78.90 % / 0.0376	78.65 % / 0.0381

Figure 11: Performance of neural networks (NN), infinite width NTKs, NTKs of varying depth on top of deep network feature matrices (NTK + $W_1^T W_1$), and Laplace kernels on top of deep network feature matrices (Laplace + $W_1^T W_1$) for SVHN classification.

We show, qualitatively, the amount of noise in the average gradient outer product estimation decreases with depth, demonstrating that features are amplified (see Fig. 12). Further, we see that the average gradient outer product closely resembles the neural feature matrix, supporting the neural feature ansatz. We also show the diagonal of the feature matrix for these experiments at various depths (see Fig. 13).

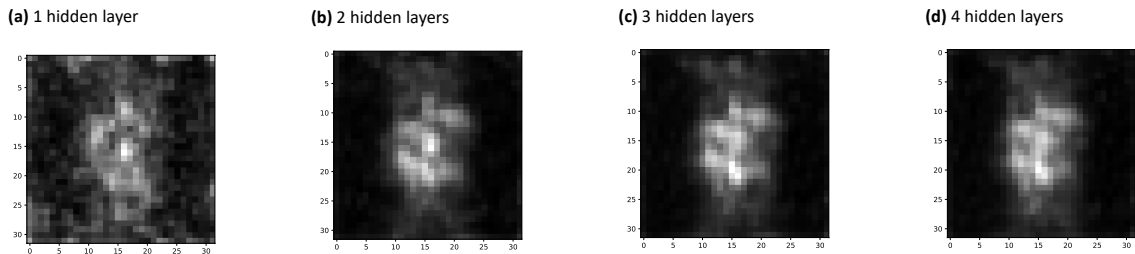


Figure 12: Centered average gradient outer product, $\sum_{i=1}^n \nabla_x \hat{f}(x_i) \nabla_x \hat{f}(x_i)^\top$, for fully-connected neural networks trained on SVHN classification.

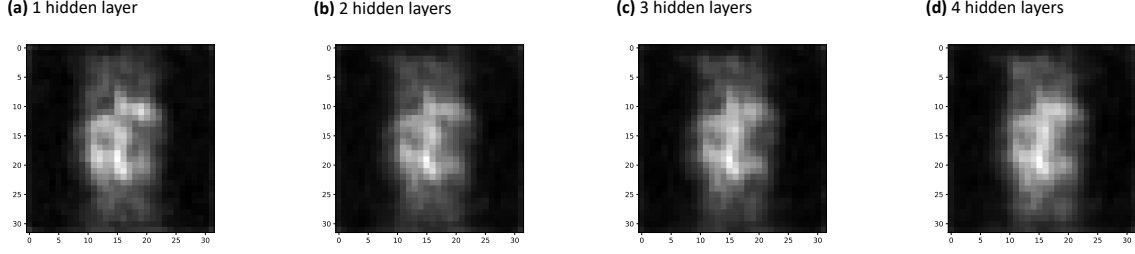


Figure 13: The feature matrix, $W_1^T W_1$, of fully-connected neural networks trained on SVHN classification.

There is also evidence of feature amplification with depth on SVHN, as the intensities of the largest 300 pixels increases relative to the remaining pixels on the diagonal with increasing depth (see Fig. 14).

Finally, we provide an additional low rank experiment to demonstrate that a Mahalanobis kernel with the neural feature matrix exceeds the performance of the neural network.

Method	Depth 1	Depth 2	Depth 3
NN	0.0829	0.0732	0.0707
NTK	0.280	0.465	0.574
NTK + $W_1^T W_1$	0.0384	0.0422	0.0428
Laplace	0.712	-	-
Laplace + $W_1^T W_1$	0.0547	0.0631	0.0605

Figure 14: Mean squared error for low rank polynomial regression with data drawn from a Gaussian distribution, $x \sim \frac{1}{4}\mathcal{N}(0, I)$, $y = x_1 x_2$, and no label noise. 1000 train and test samples were used. We compare performance for the following models: neural networks (NN), infinite width NTKs, NTKs of varying depth on top of deep network feature matrices (NTK + $W_1^T W_1$), and Laplace kernels on top of deep network feature matrices (Laplace + $W_1^T W_1$).

Lipstick			Hat			Mustache			Glasses		
	Deep Network	RFM		Deep Network	RFM		Deep Network	RFM		Deep Network	RFM
Eigenvector 1			Eigenvector 1			Eigenvector 1			Eigenvector 1		
Eigenvalue 1	115.77	2428.32	Eigenvalue 1	29.43	614.74	Eigenvalue 1	147.06	1171.10	Eigenvalue 1	131.58	1510.53
Correlation	0.999		Correlation	0.995		Correlation	0.999		Correlation	0.998	
Eigenvector 2			Eigenvector 2			Eigenvector 2			Eigenvector 2		
Eigenvalue 2	10.75	30.38	Eigenvalue 2	12.46	13.57	Eigenvalue 2	13.72	19.69	Eigenvalue 2	14.30	22.03
Correlation	0.968		Correlation	0.974		Correlation	0.983		Correlation	0.957	
Eigenvector 3			Eigenvector 3			Eigenvector 3			Eigenvector 3		
Eigenvalue 3	9.70	9.29	Eigenvalue 3	7.91	6.04	Eigenvalue 3	11.82	3.37	Eigenvalue 3	10.03	4.36
Correlation	0.982		Correlation	0.967		Correlation	0.973		Correlation	0.979	

Rosy Cheeks			5 o'clock shadow			Smiling			Necktie		
	Deep Network	RFM		Deep Network	RFM		Deep Network	RFM		Deep Network	RFM
Eigenvector 1			Eigenvector 1			Eigenvector 1			Eigenvector 1		
Eigenvalue 1	77.63	1827.43	Eigenvalue 1	104.86	2240.25	Eigenvalue 1	131.92	2508.23	Eigenvalue 1	75.45	1009.26
Correlation	0.999		Correlation	0.999		Correlation	0.999		Correlation	0.999	
Eigenvector 2			Eigenvector 2			Eigenvector 2			Eigenvector 2		
Eigenvalue 2	5.95	34.72	Eigenvalue 2	13.58	43.48	Eigenvalue 2	10.60	41.76	Eigenvalue 2	11.73	25.41
Correlation	0.973		Correlation	0.976		Correlation	0.966		Correlation	0.964	
Eigenvector 3			Eigenvector 3			Eigenvector 3			Eigenvector 3		
Eigenvalue 3	4.85	9.31	Eigenvalue 3	11.30	8.01	Eigenvalue 3	7.05	10.43	Eigenvalue 3	10.12	4.64
Correlation	0.971		Correlation	0.972		Correlation	0.990		Correlation	0.969	

Eyebrows			Goatee			Male			Blonde		
	Deep Network	RFM		Deep Network	RFM		Deep Network	RFM		Deep Network	RFM
Eigenvector 1			Eigenvector 1			Eigenvector 1			Eigenvector 1		
Eigenvalue 1	85.89	2854.74	Eigenvalue 1	102.86	1463.44	Eigenvalue 1	153.57	2355.98	Eigenvalue 1	42.32	1343.93
Correlation	0.999		Correlation	0.999		Correlation	0.999		Correlation	0.997	
Eigenvector 2			Eigenvector 2			Eigenvector 2			Eigenvector 2		
Eigenvalue 2	16.16	68.07	Eigenvalue 2	18.16	26.56	Eigenvalue 2	14.22	26.33	Eigenvalue 2	10.60	39.65
Correlation	0.976		Correlation	0.969		Correlation	0.964		Correlation	0.961	
Eigenvector 3			Eigenvector 3			Eigenvector 3			Eigenvector 3		
Eigenvalue 3	8.30	20.84	Eigenvalue 3	6.74	5.27	Eigenvalue 3	11.19	6.98	Eigenvalue 3	7.52	11.25
Correlation	0.967		Correlation	0.973		Correlation	0.979		Correlation	0.963	

Figure 15: Top three eigenvectors and corresponding eigenvalues of feature matrices of deep networks and RFMs trained for the 12 CelebA classification tasks considered in this work. Overall, we observe (1) Pearson correlation greater than 0.99 between the top eigenvectors of deep network feature matrices and RFM feature matrices and (2) a large gap between the top eigenvalue and second eigenvalue for all feature matrices. These two observations together provide further evidence that RFMs are accurately capturing the features learned by deep fully connected neural networks. In addition, we interestingly observe some cases such as hat, goatee, and blonde classification where the third eigenvector of RFM feature matrices appears visually identical to the second eigenvector of deep network feature matrices.

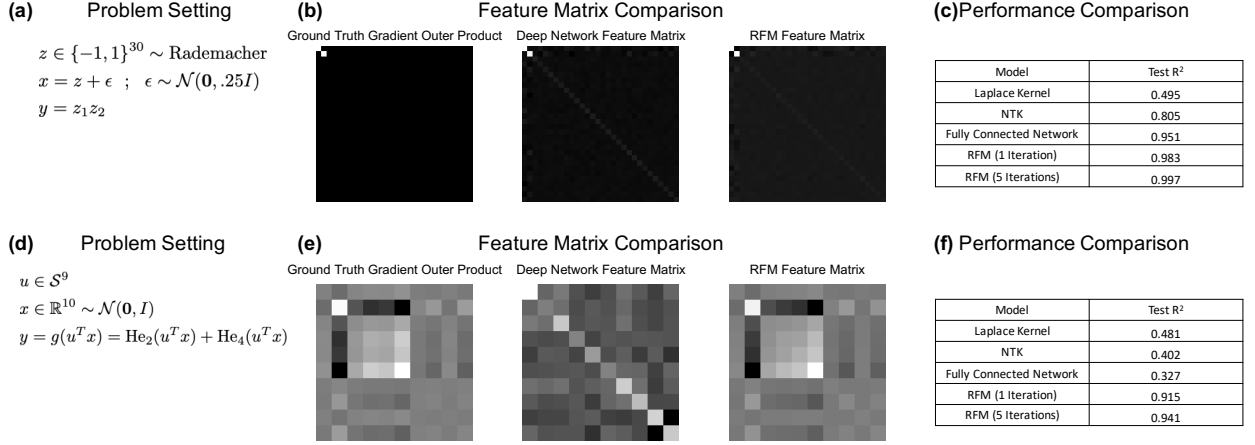


Figure 16: RFMs close the gap and surpass neural networks on low rank polynomial tasks from previous work [22, 93]. All experimental details are provided in Appendix D. (a) We consider the low rank setup from [93] in which the targets, y , are generated as a product of the first two coordinates of Rademacher random variables z . (b) Since we know the target function, we can compare the ground truth gradient outer product against the feature matrices of a trained 1 hidden layer ReLU fully connected network and a trained RFM. We observe that both models learn to select the top two coordinates. (c) The performance of RFMs and neural networks far exceeds of NTKs and Laplace kernels since these methods learn to select relevant coordinates for prediction. (d) The low rank setup from [22] in which the targets, y are generated as a function of a projection of the input x onto a 1 dimensional subspace. Here, u is on the unit sphere in 10 dimensions and He_2, He_4 denote the second and fourth probabilist’s Hermite polynomials. (e) While RFMs learn to accurately approximate the ground truth gradient outer product, fully connected networks require additional training modifications, as discussed in [22]. (f) As they learn the relevant subspace, RFMs far outperform 1 hidden layer ReLU fully connected networks, NTKs, and the Laplace kernel.

n-train	data-keyword	FT Transformer	GradientBoostingTree	RandomForest	Resnet	SAINT	XGBoost	ours	best method
4547.0	wine-quality	-	0.458	0.504	-	-	0.498	0.497	RandomForest
5457.0	isolet	-	-	-	-	-	-	0.868	ours
5734.0	cpu-act	-	0.985	0.983	-	-	0.986	0.986	XGBoost
7056.0	sulfur	-	0.806	0.859	-	-	0.865	0.913	ours
7484.0	Brazilian-houses	-	0.996	0.993	-	-	0.998	0.938	XGBoost
9625.0	Ailerons	-	0.843	0.839	-	-	0.844	0.841	XGBoost
9752.0	MiamiHousing2016	-	0.924	0.924	-	-	0.936	0.934	XGBoost
10000.0	Bike-Sharing-Demand	-	0.69	0.687	-	-	0.695	0.689	XGBoost
10000.0	california	-	0.846	0.83	-	-	0.853	0.867	ours
10000.0	diamonds	-	0.945	0.945	-	-	0.946	0.945	XGBoost
10000.0	elevators	-	0.863	0.841	-	-	0.908	0.923	ours
10000.0	fifa	-	0.663	0.655	-	-	0.668	0.653	XGBoost
10000.0	house-16H	-	0.541	0.486	-	-	0.548	0.489	XGBoost
10000.0	house-sales	-	0.884	0.871	-	-	0.887	0.883	XGBoost
10000.0	houses	-	0.84	0.829	-	-	0.852	0.864	ours
10000.0	medical-charges	-	0.979	0.979	-	-	0.979	0.979	GradientBoostingTree
10000.0	nyc-taxi-green-dec-2016	-	0.554	0.563	-	-	0.553	0.532	RandomForest
10000.0	pol	-	0.99	0.989	-	-	0.99	0.991	ours
10000.0	superconduct	-	0.905	0.909	-	-	0.911	0.911	ours
10000.0	year	-	0.271	0.241	-	-	0.282	0.303	ours
37758.0	diamonds	0.945	0.947	-	0.941	0.945	0.948	0.948	ours
50000.0	nyc-taxi-green-dec-2016	0.12	0.624	-	0.247	0.534	0.629	0.569	XGBoost
50000.0	year	0.117	0.307	-	0.119	0.289	0.307	0.334	ours

Table 2: Regression R^2 without categorical variables

n-train	data-keyword	FT Transformer	GradientBoostingTree	MLP	RandomForest	Resnet	SAINT	XGBoost	ours	best method
1787.0	wine	77.54	78.77	77.62	78.96	77.95	77.09	79.85	80.67	ours
2220.0	phoneme	85.28	86.78	84.95	88.55	86.21	85.58	86.48	88.16	RandomForest
3631.0	kdd-ipums-la-97-small	88.96	88.38	87.95	87.95	88.07	89.02	88.26	88.62	SAINT
5325.0	eye-movements	58.62	63.75	56.89	65.04	57.41	58.93	65.54	61.14	XGBoost
7057.0	pol	98.47	97.94	94.27	98.21	94.81	98.14	98.05	98.33	FT Transformer
7404.0	bank-marketing	80.42	80.27	79.18	79.82	79.37	79.09	80.44	79.73	XGBoost
9363.0	MagicTelescope	85.09	85.88	84.7	85.6	85.78	85.1	85.92	86.5	ours
9441.0	house-16H	88.16	88.2	87.78	87.8	87.5	88.16	88.83	87.78	XGBoost
10000.0	Higgs	70.62	71.08	68.86	70.76	69.44	70.72	71.42	70.73	XGBoost
10000.0	MiniBooNE	93.74	93.19	93.54	92.65	93.68	93.52	93.62	93.93	ours
10000.0	california	88.62	89.82	86.0	89.21	87.57	89.07	90.17	90.29	ours
10000.0	covertime	81.32	81.87	78.89	82.73	80.26	80.31	81.9	85.95	ours
10000.0	credit	76.53	77.22	75.99	77.28	76.1	75.99	77.38	77.66	ours
10000.0	electricity	82.0	86.16	81.04	86.14	80.86	81.77	86.83	82.93	XGBoost
10000.0	jannis	76.55	77.02	74.57	77.27	74.6	77.26	77.78	78.28	ours
40306.0	jannis	79.74	79.47	76.45	78.85	78.59	79.77	79.56	80.68	ours
50000.0	Higgs	73.13	72.55	71.15	71.98	72.39	72.75	72.83	72.44	FT Transformer
50000.0	MiniBooNE	94.34	94.14	94.32	93.53	94.44	94.32	94.43	94.97	ours
50000.0	covertime	90.69	89.76	87.43	90.59	89.39	89.53	89.74	94.1	ours

Table 3: Classification accuracy without categorical variables

n-train	data-keyword	FT Transformer	GradientBoostingTree	HistGradientBoostingTree	RandomForest	Resnet	XGBoost	ours	best method
2836.0	analcata-supreme	0.977	0.981	0.982	0.981	0.978	0.983	0.987	ours
2946.0	Mercedes-Benz-Greener-Manufacturing	0.548	0.578	0.576	0.575	0.545	0.578	0.575	GradientBoostingTree
6048.0	visualizing-soil	0.998	1.0	1.0	1.0	0.998	1.0	1.0	RandomForest
6219.0	yprop-4-1	0.037	0.056	0.063	0.095	0.021	0.08	0.072	RandomForest
7484.0	Brazilian-houses	0.883	0.995	0.993	0.993	0.878	0.998	0.906	XGBoost
9999.0	OnlineNewsPopularity	0.143	0.153	0.156	0.149	0.13	0.162	0.139	XGBoost
10000.0	Bike-Sharing-Demand	0.937	0.942	0.942	0.938	0.936	0.946	0.933	XGBoost
10000.0	SGEMM-GPU-kernel-performance	1.0	1.0	1.0	1.0	1.0	1.0	1.0	ours
10000.0	black-friday	0.379	0.615	0.616	0.609	0.36	0.619	0.612	XGBoost
10000.0	diamonds	0.99	0.99	0.991	0.988	0.989	0.991	0.991	XGBoost
10000.0	house-sales	0.891	0.891	0.89	0.875	0.881	0.896	0.891	XGBoost
10000.0	nyc-taxi-green-dec-2016	0.511	0.573	0.539	0.585	0.451	0.578	0.549	RandomForest
10000.0	particulate-matter-ukair-2017	0.673	0.683	0.69	0.674	0.658	0.691	0.662	XGBoost
37758.0	diamonds	-	0.992	0.993	-	-	0.993	0.993	ours
50000.0	SGEMM-GPU-kernel-performance	-	1.0	1.0	-	-	1.0	1.0	XGBoost
50000.0	black-friday	-	0.631	0.636	-	-	0.639	0.623	XGBoost
50000.0	nyc-taxi-green-dec-2016	-	0.636	0.585	-	-	0.648	0.589	XGBoost
50000.0	particulate-matter-ukair-2017	-	0.706	0.71	-	-	0.712	0.69	XGBoost

Table 4: Regression R^2 with categorical variables

n-train	data-keyword	FT Transformer	GradientBoostingTree	HistGradientBoostingTree	RandomForest	Resnet	SAINT	XGBoost	ours	best method
3479.0	rl	70.31	77.62	76.05	79.79	70.56	68.2	77.01	70.47	RandomForest
3522.0	KDDCup09-upselling	78.05	-	-	-	76.98	77.8	-	-	FT Transformer
3589.0	KDDCup09-upselling	-	80.36	80.61	80.02	-	-	79.56	77.24	HistGradientBoostingTree
5325.0	eye-movements	59.83	63.94	63.58	65.73	57.93	58.54	66.77	62.75	XGBoost
10000.0	compass	75.34	74.09	75.15	79.28	74.46	71.87	76.91	77.5	RandomForest
10000.0	covertypes	86.74	85.56	84.47	85.89	85.27	84.95	86.42	89.5	ours
10000.0	electricity	84.16	87.97	88.15	87.76	82.64	83.35	88.69	85.33	XGBoost
10000.0	road-safety	76.74	76.21	76.45	75.88	76.08	76.43	76.69	75.48	FT Transformer
50000.0	covertypes	93.61	93.22	92.09	93.35	92.24	92.58	93.31	95.58	ours
50000.0	road-safety	78.95	78.73	78.85	78.13	78.41	77.96	80.29	77.56	XGBoost

Table 5: Classification accuracy with categorical variables